

Finite element methods for nonlinear elliptic and parabolic problems with memory properties

Roger Van Keer

Luc Dupré

Preface

In this monograph we outline finite element methods for highly nonlinear boundary value problems of elliptic and parabolic type in 1D and 2D with memory effects. These problems arise e.g. from a recent topic in the mathematical theory of electromagnetism, viz the mathematical modelling and numerical evaluation of the electromagnetic field in magnetic materials showing hysteresis behaviour. Thus, in particular, we consider parabolic problems with *nonlocal* Neumann-BCs and we also consider the coupling of a transient 2D-problem with a vector hysteresis model.

For each of the boundary value problems (BVPs) considered, the following 3 mathematical items are dealt with:

- the variational formulation in suitable function spaces (Sobolev spaces) on the domain.
- the discretisation in the space variable by a conforming finite element method with quadratic interpolation functions, followed by a modified Crank-Nicholson finite difference method for the time discretisation.

Received by the editors January 1997 : In revised form : June 1998.

Communicated by A. Bultheel.

1991 *Mathematics Subject Classification* : 35J25, 35K20, 65N30, 78A25.

Key words and phrases : Finite elements, finite differences, partial differential equations, hysteresis.

- suitable iteration procedures devised to take into account the strongly nonlinear character of the differential equation (DE), as mentioned above. Actually, the hysteresis concerns a major difficulty in the analysis.

The fully discrete approximation schemes are validated by comparison of numerical results, obtained by means of the algorithms, with experimental values, where the latter are available.

An outline of this work is now in order. For those readers who are not familiar with finite element methods and finite difference methods, a short introduction is provided. The same holds for the basic concepts of electromagnetic fields.

In Sections 2 and 3 we consider nonlinear parabolic problems with memory in 1D and 2D respectively, using a scalar hysteresis model. In the 2D case we discuss both the cartesian and the axi-symmetric setting. In Section 4 we return to a nonlinear parabolic problem in 1D with memory, now invoking a vector hysteresis model. The same vector hysteresis model is applied in Section 5, dealing with a 2D elliptic problem. In each section we briefly state a physical problem, the mathematical modelling of which precisely leads to the respective type of BVP considered. These motivating problems all originate from the numerical evaluation of electromagnetic fields in electric machines. However, the nonlinear BVPs with memory effects dealt with in this monograph may also arise from other disciplines in engineering and physics, cf. [1] for a readable, recent account.

1 Introduction

To keep this monograph self contained to a reasonable extent, we present in this introduction some key features both of the finite element-finite difference methods used and of the hysteresis behaviour of the magnetic materials considered.

1.1 Finite Element Methods (FEMs)

When describing the basic ideas of the specific FEMs used in this text, we may restrict ourselves to two *model* problems of 2nd order elliptic problems on a bounded interval $\Omega \subset \mathbb{R}$ or a rectangle $\Omega \subset \mathbb{R}^2$ respectively, with classical Neumann boundary conditions (BCs). For the expository purpose we only consider here linear problems. The modifications required for nonlinear problems will be discussed in some detail in the specific sections where they are met. The same holds for the problems with *nonlocal* BCs. The combined finite element - finite difference methods (FEMs-FDs), used for the corresponding transient (parabolic) boundary value problems (BVPs), are dealt with in Section 1.2.

As is well known, a FEM for a BVP rests upon a proper *variational formulation* of this problem in suitable function spaces, obtained by applying Green's theorem in Sobolev spaces. This is recalled below. Throughout our work, for the sake of numerical accuracy, in the finite element discretisation of the variational problems, we shall use a *quadratic finite element mesh*. Thus, the trial and test functions will

be taken to be continuous functions on $\bar{\Omega}$, which are piecewise quadratic polynomials – piecewise with respect to the partition or triangulation of Ω in subintervals or triangles respectively. For a comprehensive account on FEMs we may refer e.g. to [2] and [3].

1.1.1 A 2nd order model problem on a bounded interval

We consider the following inhomogeneous Neumann-problem on the interval $\Omega =]0, 1[$

Find a (real valued) function $u \in H^2(\Omega)$:

$$-\frac{d}{dx} \left[p(x) \frac{du}{dx} \right] + q(x)u = f(x), \text{ a.e. in } \Omega, \quad (1.1)$$

$$p(0)u'(0) = g_1, \quad p(1)u'(1) = g_2, \quad (1.2)$$

where the data p , q and f are sufficiently regular (real) functions of x and where g_1 and g_2 are given (real) constants. (The case $q \equiv 0$ in Ω and $g_1 = g_2 = 0$, being disregarded, for the sake of uniqueness of the solution). Here $H^m(\Omega) \equiv W_2^m(\Omega)$, $m \in \mathbb{N}_0$, is the usual m th order Sobolev space on Ω , i.e.

$$H^m(\Omega) = \{u \in L_2(\Omega) \mid \text{the generalized (distributional) derivatives} \\ d^\alpha u / dx^\alpha \in L_2(\Omega), \alpha = 1, \dots, m\} \quad (1.3)$$

First step: Variational formulation in $H^1(\Omega)$

We multiply both sides of (1.1) with an arbitrary test function $v \in H^1(\Omega)$ and integrate over Ω . Next, we use the formula of integration by parts in $H^1(\Omega)$, i.e.

$$\int_0^1 \frac{dw}{dx} v dx = w(1)v(1) - w(0)v(0) - \int_0^1 w \frac{dv}{dx} dx, \quad \forall v, w \in H^1(\Omega). \quad (1.4)$$

Invoking the BCs (1.2), the solution u of (1.1)-(1.2), is seen to be a solution of the following variational problem (*continuous* problem)

Find $u \in H^1(\Omega)$:

$$a(u, v) = l(v), \forall v \in H^1(\Omega) \quad (1.5)$$

where

$$a(u, v) = \int_0^1 \left(p \frac{du}{dx} \frac{dv}{dx} + quv \right) dx, \quad (1.6)$$

$$l(v) = \int_0^1 f v dx - g_1 v(0) + g_2 v(1). \quad (1.7)$$

By the well known Lax Milgram lemma, the existence of a unique, stable, solution of (1.5) is guaranteed when

$$\begin{cases} p, q \text{ and } f \in L_\infty(\Omega), \\ \exists p_0 > 0 \text{ (constant)} : p \geq p_0, \text{ a.e. in } \Omega, q \geq 0 \text{ a.e. in } \Omega. \end{cases} \quad (1.8)$$

Moreover, (1.5) is seen to be formally equivalent to the problem (1.1)-(1.2). [Notice that, due to the continuous embedding $H^1(\Omega) \hookrightarrow C^0(\bar{\Omega})$, the trace $(\gamma v)(0)$ of $v \in H^1(\Omega)$ in the boundary point $x = 0$ may simply be written as $v(0)$, etc.]

Second step: Internal approximation of (1.5) – particular choice of a finite element space

The Galerkin idea of the internal approximation of (1.5) is first to introduce a suitable function space X_h ,

$$X_h \subset H^1(\Omega), \quad \dim X_h < +\infty, \quad (1.9)$$

and then to rephrase the variational problem in that space. This leads to the *discrete* problem

$$\text{Find } u_h \in X_h : a(u_h, v) = l(v), \forall v \in X_h \quad (1.10)$$

In standard FEMs, X_h is chosen to be a space of continuous functions on $\bar{\Omega}$, which are piecewise polynomials of some low degree – piecewise with respect to a partition of $\bar{\Omega}$ in *elements*. To be specific, divide $[0, 1]$ in n equal subintervals (elements) by $0 = x_0 < x_2 < \dots < x_{2n-2} < x_{2n} = 1$, and let

$$X_h = \left\{ v \in C^0([0, 1]) \mid v \text{ is a quadratic polynomial in each element } [x_{2k-2}, x_{2k}], 1 \leq k \leq n \right\}, \quad \left(h = \frac{1}{n} = \text{mesh parameter} \right). \quad (1.11)$$

To identify a suitable basis of X_h , we consider an internal node in each element, the midpoint say, denoted by x_{2k-1} , $k = 1, \dots, n$, cf. Fig. 1.1. The *cardinal basis* of X_h is then defined by

$$(\varphi_i)_{i=0}^{2n} \subset X_h, \quad \varphi_i(x_j) = \delta_{ij}, \quad \text{for } i \text{ and } j = 0, \dots, 2n. \quad (1.12)$$

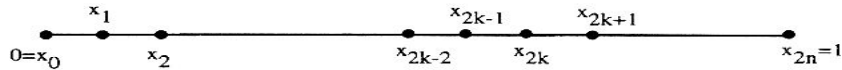


Figure 1.1: A uniform FE-mesh

Notice that φ_i isn't identically zero only in those elements that contain the node i . Typical basis functions are depicted in Fig.1.2.

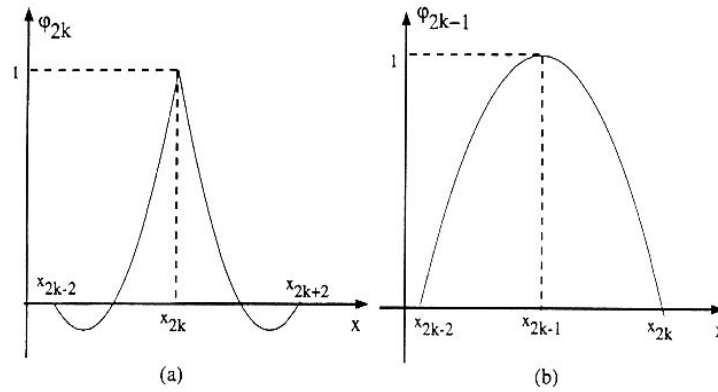


Figure 1.2: (a) The basis function φ_{2k} on its support (b) The basis function φ_{2k-1} on its support

Third step: Algebraic form of (1.10)

First, taking $v = \varphi_i$, $i = 0, 1, \dots, 2n$ in (1.10), and next, inserting

$$u_h = \sum_{j=0}^{2n} c_j \varphi_j, \quad (1.13)$$

we end up with the following algebraic system:

Find the column matrix $[C] \equiv [c_0, \dots, c_{2n}]^T \in \mathbb{R}^{2n+1}$:

$$[K][C] = [F], \quad (1.14)$$

where the stiffness matrix $[K] \in \mathbb{R}^{2n+1} \times \mathbb{R}^{2n+1}$ and the force matrix $[F] \in \mathbb{R}^{2n+1} \times 1$ are defined as

$$[K] = [K_{ij}]_{0 \leq i, j \leq 2n} \text{ and } [F] = [F_0, \dots, F_{2n}]^T \quad (1.15)$$

with

$$K_{ij} = a(\varphi_i, \varphi_j), F_i = l(\varphi_i). \quad (1.16)$$

The matrix K is symmetric. Due to the particular choice of the basis functions, K is seen to have a band structure with bandwidth 5. Moreover, the conditions (1.8) guarantee K to be positive definite and hence also non-singular. [In fact, the Lax Milgram lemma automatically implies the problem (1.10), and, equivalently, the algebraic problem (1.14), to have a unique solution].

1.1.2 A 2nd order model problem on a rectangle

We consider the following Neumann-problem on a rectangle $\Omega \subset \mathbb{R}^2$.

Find a (real valued) function $u \in H^2(\Omega)$:

$$-\operatorname{div}(p(x)\operatorname{grad}u) + qu = f(x), \text{ a.e. in } \Omega \quad (1.17)$$

$$p \frac{\partial u}{\partial n} = g(x), \text{ a.e. on } \partial\Omega \quad (1.18)$$

where $x = [x_1, x_2]$ and where p, q, f and g are sufficiently regular given functions of x (now the case $q \equiv 0$ in Ω , $g \equiv 0$ on $\partial\Omega$ being excluded). Here the Sobolev space $H^m(\Omega) \equiv W_2^m(\Omega)$, $m \in \mathbb{N}_0$, is given by

$H^m(\Omega) = \{u \in L_2(\Omega) \mid \text{the generalized (distributional) derivatives}$

$$D^\alpha u = \frac{\partial^{|\alpha|}}{\partial x_1^{\alpha_1} \partial x_2^{\alpha_2}} \in L_2(\Omega),$$

$$\text{for all } \alpha = [\alpha_1, \alpha_2] \in \mathbb{N}^2, \text{ with } |\alpha| \leq m, |\alpha| = \alpha_1 + \alpha_2 \}. \quad (1.19)$$

Moreover, in (1.18), $\frac{\partial u}{\partial n} \in L_2(\Omega)$ denotes the generalized normal derivative of u , i.e.

$$\frac{\partial u}{\partial n} = \left(\gamma \frac{\partial u}{\partial x_1}\right) n_1 + \left(\gamma \frac{\partial u}{\partial x_2}\right) n_2,$$

$$[n_1, n_2] = \bar{n} \equiv \text{the outward unit normal vector to } \partial\Omega \quad (1.20)$$

where $\gamma: H^1(\Omega) \rightarrow L_2(\partial\Omega)$ is the usual trace operator.

First step: Variational formulation in $H^1(\Omega)$

We now lean upon Green's formula, viz

$$\int_{\Omega} \frac{\partial w}{\partial x_i} v dx = \int_{\partial\Omega} (\gamma w) (\gamma v) n_i ds - \int_{\Omega} w \frac{\partial v}{\partial x_i} dx, \quad i = 1, 2, \quad \forall v \text{ and } w \in H^1(\Omega) \quad (1.21)$$

to arrive at

$$\text{Find } u \in H^1(\Omega) : a(u, v) = l(v), \forall v \in H^1(\Omega), \quad (1.22)$$

where

$$a(u, v) = \int_{\Omega} [(p \operatorname{grad} u) \operatorname{grad} v + quv] dx, \quad (1.23)$$

$$l(v) = \int_{\Omega} f v dx + \int_{\partial\Omega} g (\gamma v) ds. \quad (1.24)$$

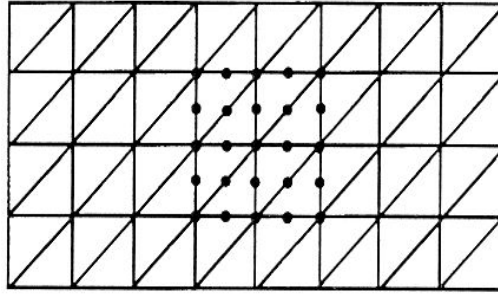
Under the conditions (1.8) the Lax Milgram lemma again guarantees the existence of a unique solution of (1.17)-(1.18).

Second step: Internal approximation of (1.17)-(1.18) – particular choice of a finite element space

To construct a finite dimensional subspace X_h of $H^1(\Omega)$, we may consider a partition τ_h of $\bar{\Omega}$ in triangles (elements) K . For the conventions tacitly made in such a triangulation, see e.g. [2].

We take

$$X_h = \{v \in C^0(\bar{\Omega}) \mid v \text{ is a quadratic polynomial in each element } K \in \tau_h\} \quad (1.25)$$

Figure 1.3: A uniform triangulation of $\bar{\Omega}$

(h = mesh parameter = length of the longest side in τ_h .)

To identify a suitable basis of X_h , recall that a quadratic polynomial on a triangle K is uniquely defined by prescribing its value in the 3 vertices of K together with its value in 3 side points, the midpoints of the sides of K , say. Let $[x_1^i, x_2^i]$, $1 \leq i \leq N$, be the set of all nodes, i.e. the set of all vertices of all triangles $K \in \tau_h$ and of all midpoints of all corresponding sides. The *cardinal basis* of X_h is defined by:

$$(\varphi_i)_{i=1}^N \subset X_h, \quad \varphi_i(x_1^j, x_2^j) = \delta_{ij} \text{ for } i \text{ and } j = 1, \dots, N. \quad (1.26)$$

The support of φ_i is the union of the triangles sharing the node i . In particular, when i refers to a side midpoint not belonging to $\partial\Omega$, there are 2 triangles sharing that node. For a vertex node i not lying on $\partial\Omega$, φ_i is graphically represented by a 6-sided, quadratically curved pyramid resting upon the 6 triangles that share the node i , its top lying vertically above that node at the height 1.

Third step: Algebraic form of (1.10)

The equivalent algebraic version of the discrete problem (1.10) is obtained similarly as in (1.14). A major task is to *construct* the stiffness matrix K and the force matrix F . In practice this is performed by splitting the involved integrals over Ω and $\partial\Omega$ into contributions coming from the individual elements $K \in \tau_h$ and their eventual sides on $\partial\Omega$ and to reduce the *element computations* to a fixed *master element* \hat{K} and its sides by means of an affine, invertible transformation. In most cases the integrations over \hat{K} and its sides may be simplified considerably by using appropriate quadrature rules.

1.2 Finite Difference Methods (FDMs)

For the transient BVPs of the parabolic type, encountered in this work, we will apply a combined FEM-FDM. Beginning with the space discretisation by a FEM, we arrive at an initial value problem (IVP) for a system of 1st order ODEs for the time varying nodal values $c_i(t)$ of the approximate unknown $u_h(x, t)$ in the nodes $x = x_i$, $1 \leq i \leq N$, of the FE-mesh. This IVP is solved numerically by a FDM. We

are led to a recurrent set of algebraic systems to be solved at each subsequent time point t_k of a time partitioning, cf. Section 7.4 in [4].

Below we illustrate the basic ideas for a simple model problem in 1D, which again is chosen to be linear. The modifications required when dealing with a nonlinear problem are discussed in some detail in the specific sections where these problems are met.

A model parabolic problem

We look for a smooth function $u(x, t)$, $0 \leq x \leq 1$, $t \geq 0$, which obeys, in a weak sense, the DE

$$\frac{\partial u}{\partial t} = \kappa \frac{\partial^2 u}{\partial x^2}, 0 < x < 1, t > 0, \quad (1.27)$$

along with the BCs

$$\kappa u'(0, t) = g_1(t), \quad \kappa u'(1, t) = g_2(t), t > 0, \quad (1.28)$$

and the IC

$$u(x, 0) = u_0(x), 0 < x < 1. \quad (1.29)$$

Here g_1 and g_2 are given, sufficiently regular functions of time; u_0 is a given, sufficiently regular function of x and $\kappa > 0$ is a given constant (e.g. a diffusion parameter).

First step: Variational formulation

Treating the time variable t as a parameter and proceeding similarly as above, we arrive at the following variational formulation of the problem (1.27)-(1.29):

Find a function $u(x, t)$, which has the properties that $u(\cdot, t) \in H^1(\Omega)$ and $\frac{\partial u}{\partial t}(\cdot, t) \in L_2(\Omega)$ for each $t > 0$ and which obeys:

$$\left(\frac{\partial u}{\partial t}, v\right) + \kappa \left(\frac{\partial u}{\partial x}, \frac{dv}{dx}\right) = -g_1(t)v(0) + g_2(t)v(1), t > 0, \forall v \in H^1(\Omega), \quad (1.30)$$

along with the IC (1.29).

Here, for brevity, Ω denotes again the open interval $]0, 1[$, and (\cdot, \cdot) denotes the $L_2(\Omega)$ -inner product.

Second step: Semi-discrete (time continuous) approximation by a FEM

Retaining the space X_h , (1.11), we approximate the problem above by

Find a function $u_h(x, t)$, with $u_h(\cdot, t)$ and $\frac{\partial u_h}{\partial t}(\cdot, t) \in X_h$ for each $t > 0$, which obeys

$$\left(\frac{\partial u_h}{\partial t}, v\right) + \kappa \left(\frac{\partial u_h}{\partial x}, \frac{dv}{dx}\right) = -g_1(t)v(0) + g_2(t)v(1), t > 0, \forall v \in X_h, \quad (1.31)$$

along with

$$u_h(x, 0) = u_0^h(x), \quad (1.32)$$

where $u_0^h \in X_h$ is an appropriate approximation of u_0 (for instance the $L_2(\Omega)$ -projection of u_0 on X_h). When $u_0 \in C^0(\bar{\Omega})$, we may take u_0^h to be the piecewise Lagrange interpolant of u_0 in the FE-mesh. Denoting

$$u_h(\cdot, t) = \sum_{i=0}^{2n} c_i(t) \varphi_i, \quad t \geq 0, \quad (1.33)$$

and

$$u_0^h = \sum_{i=0}^{2n} b_i \varphi_i, \quad (1.34)$$

we may rewrite (1.31)-(1.32) as the following IVP:

Find $[C(t)] \equiv [c_0(t), c_1(t), \dots, c_{2n}(t)]^T$ which obeys

$$[M] \frac{d[C]}{dt} + [K][C] = [L], \quad (1.35)$$

$$[C(0)] = [B] \equiv [b_0, b_1, \dots, b_{2n}]^T. \quad (1.36)$$

Here, the mass matrix $[M]$, the stiffness matrix $[K]$ and the force matrix $[L]$ read

$$[M] = [M_{ij}]_{0 \leq i, j \leq 2n}, \quad M_{ij} = (\varphi_i, \varphi_j), \quad (1.37)$$

$$[K] = [K_{ij}]_{0 \leq i, j \leq 2n}, \quad K_{ij} = \kappa \left(\frac{d\varphi_i}{dx}, \frac{d\varphi_j}{dx} \right), \quad (1.38)$$

and

$$[L] = [-g_1(t), 0, 0, \dots, 0, g_2(t)]^T \quad (1.39)$$

respectively, where for the latter matrix the definition relation (1.12) is explicitly used.

Third step: θ -family of finite difference schemes (cf. Section 7.4 in [4])

Let Δt be a time step and let $t_k = k \cdot \Delta t$, $k \in \mathbb{N}$, be the corresponding equidistant time points. Let moreover $\theta \in [0, 1]$ be a parameter. We define an approximation

$$[\tilde{C}^{(k)}] \simeq [C(t_k)], \quad k = 1, 2, \dots \quad (1.40)$$

by means of a recurrent set of algebraic systems, viz

$$\begin{aligned} [M] \frac{[\tilde{C}^{(k)}] - [\tilde{C}^{(k-1)}]}{\Delta t} + [K](\theta[\tilde{C}^{(k)}] + (1 - \theta)[\tilde{C}^{(k-1)}]) = \\ \theta[L(t_k)] + (1 - \theta)[L(t_{k-1})], \quad k = 1, 2, \dots \end{aligned} \quad (1.41)$$

starting with

$$[\tilde{C}^{(0)}] = [C(0)] = [B] \quad (1.42)$$

When useful, we may approximate $[C(t)]$ for $t_{k-1} < t < t_k$ by means of linear interpolation between $[\tilde{C}^{(k-1)}]$ and $[\tilde{C}^{(k)}]$.

The coefficient matrix $[M+K\theta\Delta t]$ resulting from (1.41) is symmetric and positive definite and thus also non-singular. Notice that for $\theta = 0$ and $\theta = 1$ we get the explicit and the implicit Euler scheme, respectively. The choice $\theta = \frac{1}{2}$ leads to the Crank-Nicholson scheme, which, we recall, is unconditionally stable and shows $O((\Delta t)^2)$ -accuracy (whereas, the two Euler-schemes give only $O(\Delta t)$ -accuracy, the explicit scheme being moreover only conditionally stable).

1.3 Basic equations in electromagnetism

1.3.1 Maxwell equations and constitutive laws

It is well known that in electromagnetic field theory the magnetic field \bar{H} [A/m], the electric field \bar{E} [V/m] and the magnetic induction \bar{B} [T] are connected by the Maxwell equations [5]:

$$\text{rot}\bar{H} = \bar{J} + \frac{\partial\bar{D}}{\partial t}, \quad (1.43)$$

$$\text{rot}\bar{E} = -\frac{\partial\bar{B}}{\partial t}, \quad (1.44)$$

$$\text{div}\bar{B} = 0. \quad (1.45)$$

Here \bar{J} is the electric current density, while \bar{D} is the electric flux density, itself related to the electric charge density ρ [C/m³] by

$$\text{div}\bar{D} = \rho, \quad (1.46)$$

In general, ρ and \bar{J} are given quantities, while \bar{D} , \bar{H} , \bar{E} and \bar{B} are unknown vector fields. In addition to these Maxwell equations 3 constitutive laws have to be imposed, viz

$$\bar{B} = \bar{B}(\bar{H}) \quad (1.47)$$

$$\bar{J} = \bar{J}(\bar{E}) \quad (1.48)$$

$$\bar{D} = \bar{D}(\bar{E}) \quad (1.49)$$

In this monograph, the relation (1.48) will be assumed to be linear,

$$\bar{J} = \sigma\bar{E} \quad (1.50)$$

where σ [S/m] is the electrical conductivity. Moreover, as capacity effects may be neglected in this work, ρ and $\frac{\partial\bar{D}}{\partial t}$ may be taken to be zero and thus (1.49) may be disregarded. For the problems considered in this text, the constitutive relation (1.47) is a strongly nonlinear one, corresponding to the memory properties of the material ('hysteresis properties'):

$$\bar{B} = \bar{B}(\bar{H}, \bar{H}_{past}) \quad (1.51)$$

Here, the dependence on the past values of the magnetic field vector ('memory') is denoted by \bar{H}_{past} , for shorthand. The complex form of this constitutive relation will constitute the major difficulty in the evaluation of the electromagnetic field. To illustrate the complexity of this relation, in the next subsection, we briefly discuss some experimentally observed properties, for the simplified case that the magnetic field vector \bar{H} and the magnetic induction vector \bar{B} are uni-directional (their magnitude being denoted by H and B respectively).

1.3.2 Hysteresis behaviour

In order to build models of the magnetic hysteresis phenomenon, we will begin with an analysis of experimental magnetisation curves, giving B as a function of H (and of H_{past}), and we point out their fundamental characteristic features. These properties are discussed theoretical in great depth by Mayergoyz in [14]. From this reference text we adopt some terminology. First, we notice that B is not a *single valued* function of H , precisely due to the hysteresis. As a consequence, in the BH -plane a *cycle* or *loop* is observed. Next, a *limit cycle* is obtained as that BH -curve where H varies from H_{max} to $-H_{max}$ and back to H_{max} when H_{max} tends to infinity. Moreover, when the time varying magnetic field shows local extrema *minor loops* inscribed in larger BH -loops will occur.

Symmetry property

A property of almost every magnetic material is the symmetry with respect to the origin ($H=0, B=0$) of the BH -curves occurring for opposite evolutions, see Fig.1.4, i.e. when $H(t)$ is symmetric with respect to the origin,

Nonlinearity and memory

The detailed relation between the magnetic induction B and the magnetic field strength H in electrical steel is very complex. However, some specific properties may be observed. As shown in Fig.1.4, the relation between B and H is strongly nonlinear and non single valued. Moreover, each point within the limit cycle may be reached in various ways. One of the most important properties of these nonlinearities is that the relation between B and H at each time point depends on the excitation enforced to the material in the past. The material is said to have a memory in which the history is stored. It is clear that the extreme values of H have an important influence on the BH -characteristic.

We also observe that, when a minor order loop is closed, the BH -characteristic behaves as if the minor order loop has never existed. The minor order loop is evaded from the memory.

Accommodation

Experiments also show that hysteresis loop are often preceded by some stabilisation process. This means, for instance, that when the magnetic field changes

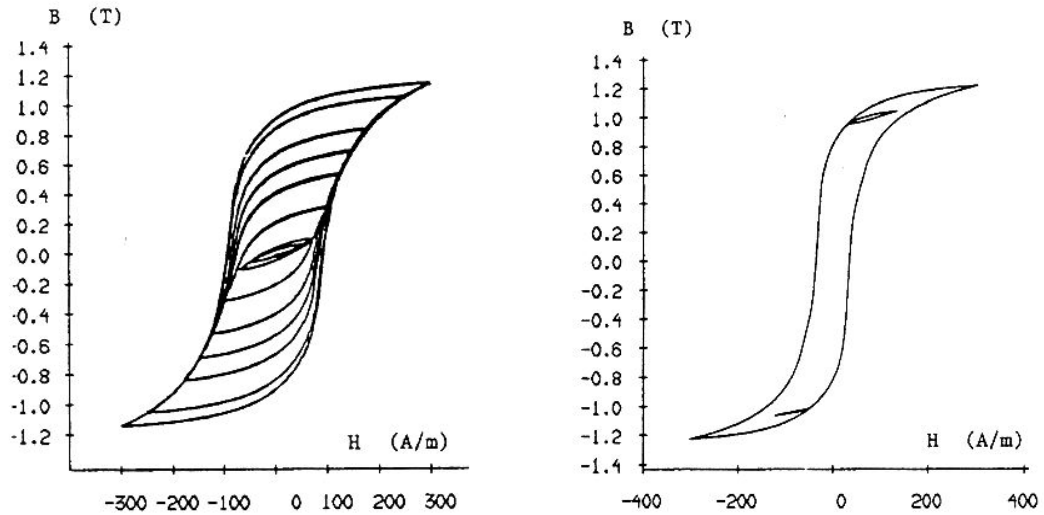


Figure 1.4: *Symmetry, Non linearity and* Figure 1.5: *Evading a minor order loop memory property*

from one time-periodic variation to another, the magnetic induction B also obtains a new time-periodic variation after some transients. Thus, a considerable number of periods may be required before a stable minor loop is achieved, see Fig.1.6. This stabilisation process is called the reptation or accommodation process. In some cases the accommodation process isn't negligible, so that it must be modeled.

Noncongruency

Finally, in Fig.1.7, a measured BH -relation is given with five minor order loops. Each minor order loop is enclosed by the same minimum and maximum value for the magnetic field strength H , but corresponds with a different induction level B . We see that these minor order loops are non-congruent.

2 1D Nonlinear Parabolic Problems with a scalar hysteresis model

2.1 A motivating physical problem and its mathematical model

The evaluation of the electromagnetic losses in electrical machines is based upon a magnetodynamic model for one lamination of the material, see Fig.2.1, where the thickness $2d$ of the lamination is very small relative to its width b . This model starts from the well known Maxwell equations, (1.43), (1.44), (1.46) and (1.45).

Throughout the lamination, which is assumed to be isotropic, the time dependent flux reads $\bar{\phi} = \phi \bar{1}_z$ (per unit length in the y -direction), with

$$\phi = \frac{1}{b} \int_{-d}^d dx \int_{-\frac{b}{2}}^{\frac{b}{2}} \bar{B} \cdot \bar{1}_z dy. \quad (2.1)$$

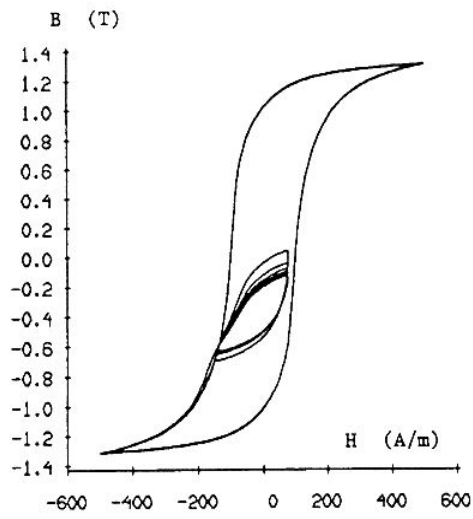


Figure 1.6: *Accommodation*

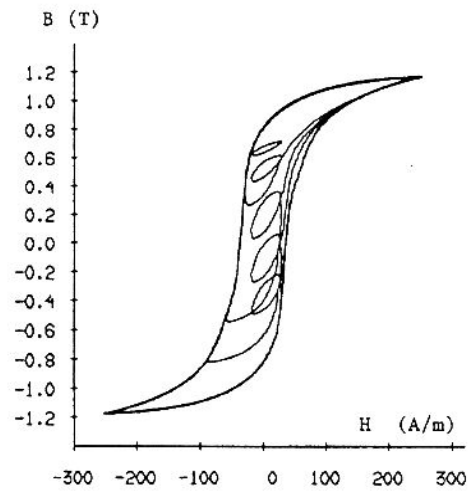


Figure 1.7: *Non-congruency*

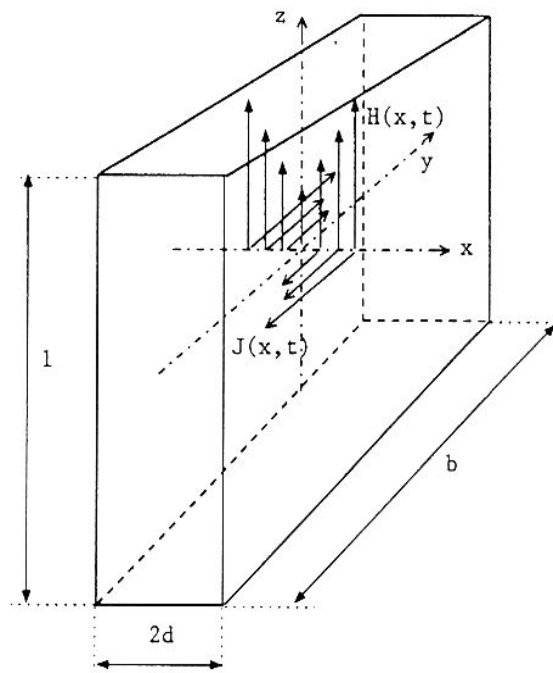


Figure 2.1: *Magnetodynamic model of one lamination*

Neglecting the end effects, as $d \ll b$, and taking into account the isotropy as well as the symmetry in the lamination, we have

$$\bar{H} = H(x, t)\bar{1}_z = H(-x, t)\bar{1}_z, \quad (2.2)$$

$$\bar{B} = B(x, t)\bar{1}_z = B(-x, t)\bar{1}_z, \quad (2.3)$$

$$\bar{J} = J(x, t)\bar{1}_y = -J(-x, t)\bar{1}_y. \quad (2.4)$$

Finally, invoking the constitutive relation (1.50) we arrive at

$$\frac{1}{\sigma} \frac{\partial^2 H}{\partial x^2} = \frac{\partial B}{\partial t}, \quad 0 < x < d, \quad t > 0. \quad (2.5)$$

This differential equation (DE) must be completed with the appropriate boundary conditions (BCs) and initial conditions (ICs), viz

$$\frac{\partial H(x=0, t)}{\partial x} = 0, \quad \frac{\partial H(x=d, t)}{\partial x} = \frac{\sigma}{2} \frac{d\phi}{dt} \quad (2.6)$$

and

$$H(x, t=0) = 0. \quad (2.7)$$

The first BC reflects the symmetry in the lamination. The second BC follows when combining (2.5) with the symmetry and with the definition of the flux $\phi(t)$, (2.1), through the lamination. Finally, the IC (2.7) corresponds to the demagnetized state of the material.

To obtain a well posed boundary value problem (BVP) for $H(x, t)$, B must be eliminated from (2.5), by means of the material properties. For this purpose, in the next section we lean upon a suitable hysteresis theory, more precisely a *rate independent* and next a *rate dependent Preisach* model.

The aim is to determine the BH -relation from this mathematical model, as this relation will allow us to evaluate the iron losses, during a time interval $[t_1, t_2]$, with length equal to an integer multiple of the period of the enforced magnetic field $H_b(t)$ or enforced magnetic induction $B_a(t)$, according to the formula

$$E = \int_{t_1}^{t_2} H_b(t) \frac{dB_a}{dt} dt \quad (2.8)$$

where

$$B_a(t) = \frac{\phi(t)}{2d}, \quad (2.9)$$

$$H_b(t) = H(x=d, t). \quad (2.10)$$

In practice two types of problems may occur: either the average flux $B_a(t)$ in the lamination is enforced, from which the magnetic field strength $H_b(t)$ at the surface of the lamination must be derived, or vice versa.

2.2 Classical Preisach model versus rate-dependent Preisach model

In the Preisach model, the material is assumed to consist of small elementary dipoles. We first discuss the basic properties of such a dipole and next we comment on the Preisach model itself.

2.2.1 Behaviour of the elementary Preisach dipole

The elementary dipoles, composing the ferromagnetic material, are characterized by two parameters, namely *the switching fields* α and β , entering the Preisach model, [6].

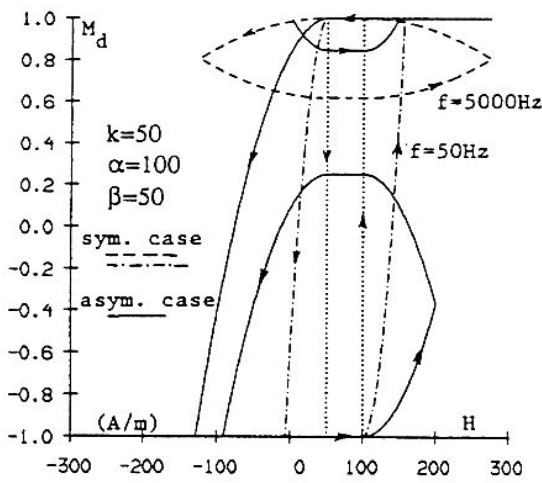


Figure 2.2: (M_d, H) -characteristics

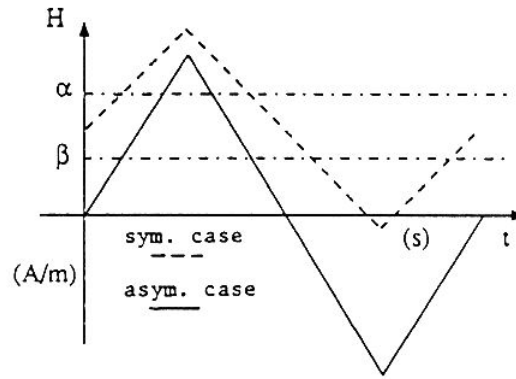


Figure 2.3: Enforced $H(t)$

In the classical (rate independent) Preisach model (CPM) the magnetisation M_d of the dipole only takes the value $+1$ or -1 , see Fig.2.2 (dotted line). Explicitly,

$$M_d = \begin{cases} +1 & : H(t) > \alpha \text{ or } (\beta < H < \alpha \text{ and } H_{last} > \alpha) \\ -1 & : H(t) < \beta \text{ or } (\beta < H < \alpha \text{ and } H_{last} < \beta) \end{cases} \quad (2.11)$$

Here H_{last} is the last extreme value kept in memory outside the interval $[\beta, \alpha]$. Thus the CPM is rate-independent.

In the rate dependent Preisach model (RPM) of [7] the dipoles are assumed to switch at a *finite* rate, proportional to the difference between the local magnetic field $H(t)$ and the elementary loop switching fields α and β . The factor of proportionality, denoted by k_d , is a material parameter. Explicitly, the evolution in time of the magnetisation M_d is given by

$$\frac{dM_d}{dt} = \begin{cases} k_d(H(t) - \alpha) & , \text{ if } H(t) > \alpha \text{ and } M_d < +1 \\ k_d(H(t) - \beta) & , \text{ if } H(t) < \beta \text{ and } M_d > -1 \\ 0 & , \text{ in the other cases} \end{cases} \quad (2.12)$$

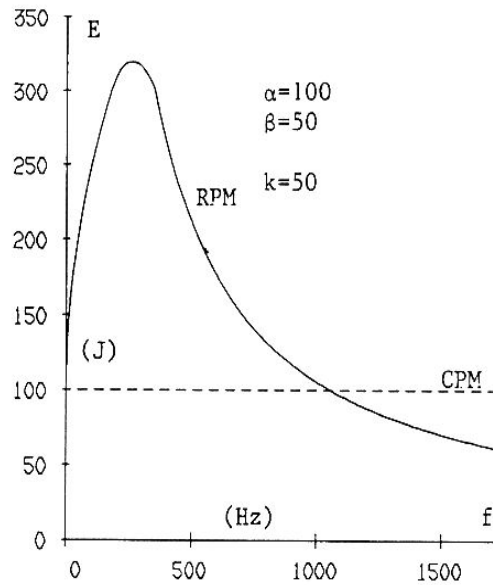


Figure 2.4: *Frequency dependency of the area enclosed*

To give an idea of the (M_d, H) -characteristic of one dipole in the RPM, we consider two relevant examples.

Example 1 (Symmetric case)

For the imposed magnetic field $H(t)$, represented by the dashed line in Fig.2.3, the corresponding (M_d, H) -loops are shown in Fig.2.2 (dashed and dash-dotted). As may be observed from Fig.2.2, the dipole can switch on completely for sufficiently low frequency, while this is no longer the case for higher frequencies.

The area enclosed by the (M_d, H) -loop during one cycle is given in Fig.2.4 as a function of the frequency, for the indicated set of data. Below a first critical frequency $f_{k,1}$, the extra enclosed area in comparison with the case of the CPM is proportional to \sqrt{f} . Above a second critical frequency $f_{k,2}$, the total area is proportional to $\frac{1}{f}$ and may become smaller than the classical area $2(\alpha - \beta)$. In the latter case the Preisach dipole does no longer switch completely from $+1$ to -1 and from -1 to $+1$.

Example 2 (Asymmetric case)

A more complex situation results for the imposed magnetic field, represented by the solid line in Fig.2.3. Due to the asymmetry of the field strength relative to the α - β parameters, the corresponding (M_d, H) -characteristics are asymmetric as well, as shown in Fig.2.2 (solid line).

2.2.2 Material characterisation

The relative density of the Preisach dipoles is represented by the distribution function $P(\alpha, \beta)$, cf. [6] and [7]. Correspondingly, the induction $B(H(t), H_{past}(t))$ takes

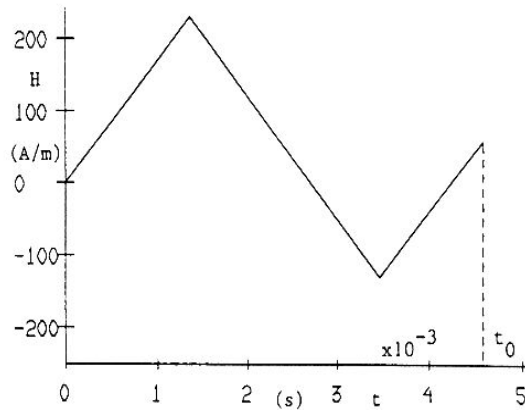


Figure 2.5: The variation of the magnetic field H in the interval $[0, t_0]$

the following form in the Preisach model:

$$B(H(t), H_{past}(t)) = \frac{1}{2} \int_{-H_m}^{H_m} d\alpha \int_{-H_m}^{\alpha} d\beta \eta(\alpha, \beta, t) P(\alpha, \beta). \quad (2.13)$$

Here, $P(\alpha, \beta)$ is assumed to be negligible small when either $\alpha > H_m$ or $\beta < -H_m$, where H_m is directly obtained from the experimental evaluation of P . Moreover $\eta(\alpha, \beta, t)$ is the value at the time t of the magnetisation M_d for the dipole with the parameters α and β . From (2.11) or (2.12), $\eta(\alpha, \beta, t)$ obviously depends on $H(t)$ and $H_{past}(t)$. Of course, this leads to the induction B to depend upon the magnetic field $H(t)$ and its history $H_{past}(t)$.

To illustrate in a *theoretical* way, the difference between the CPM and the RPM, we consider the variation of the magnetic field H as shown in Fig.2.5 for a chosen time interval $[0, t_0]$. The two models are compared on two levels: the function η in the (α, β) -plane and the BH -relation obtained by (2.13).

As mentioned above, in the CPM, $\eta(\alpha, \beta, t)$ only takes the values $+1$ or -1 . The region $(-H_m < \alpha < H_m, -H_m < \beta < \alpha)$ is divided into two subregions S^+ and S^- where $\eta(\alpha, \beta, t)$ equals $+1$ and -1 respectively. The interface between S^- and S^+ is determined by $H(t)$ and $H_{past}(t)$, as described in detail in [6]. Fig.2.6 shows the function η at time point $t = t_0$.

For the CPM, (2.13) becomes:

$$B(H(t), H_{past}(t)) = \frac{1}{2} \int_{S^+} d\alpha d\beta P(\alpha, \beta) - \frac{1}{2} \int_{S^-} d\alpha d\beta P(\alpha, \beta). \quad (2.14)$$

More generally, when the field strength H varies monotonously in time, the variation of the induction B , in absolute value, is given by:

$$\Delta B(H(t), H_{past}(t)) = \int_{D_s} d\alpha d\beta P(\alpha, \beta), \quad (2.15)$$

where D_s is the region in the (α, β) -plane in which the dipoles switch from one polarisation to the opposite one.

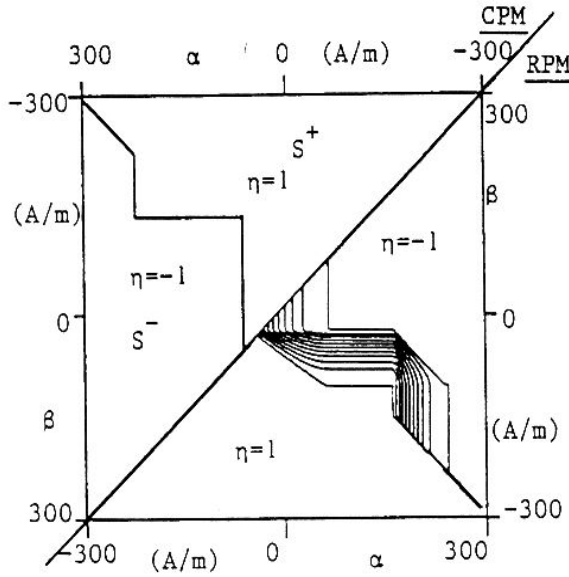


Figure 2.6: *Typical Preisach diagram for the CPM and for the RPM at time point $t = t_0$ when considering the H -variation in Fig.2.5*

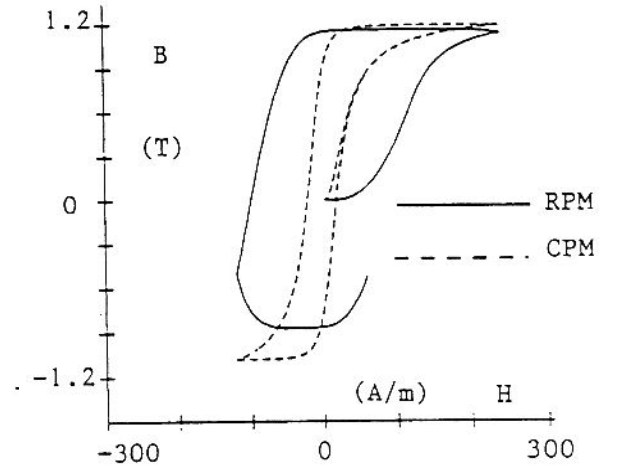


Figure 2.7: *BH relation obtained by the CPM and the RPM when considering the H -variation in Fig.2.5*

In the RPM however, $\eta(\alpha, \beta, t)$ varies (at each fixed time t) within the whole range from -1 to $+1$, according to (2.12). Now, the function η can be visualized for each time point in the (α, β) -plane using η -isolines. Fig.2.6 shows the η -isolines for the time point $t = t_0$.

Finally, using (2.13), we obtain for the RPM the BH -relation given by the full line in Fig.2.7, while the CPM results in the BH -relation in dashed line. These BH -relations correspond to the time interval $[0, t_0]$ in Fig.2.5.

2.2.3 Relation between $\frac{dB}{dt}$ and H

In view of the magnetodynamic model, $\frac{\partial B}{\partial t}$ must be related to the magnetic field $H(t)$, both for the CPM and for the RPM. In the former case one simply has

$$\frac{\partial B}{\partial t} = \frac{\partial B}{\partial H} \frac{\partial H}{\partial t} \equiv \mu_d(H(t), H_{past}(t)) \frac{\partial H}{\partial t}, \quad t > 0, \quad (2.16)$$

Here, the introduced function μ_d is the 'differential permeability' of the magnetic material. It can be derived numerically from the Preisach model using (2.13), the latter making evident the dependency of μ_d on $H(t)$ and $H_{past}(t)$.

In the RPM however, (2.13) combined with (2.12), written out for $\eta(\alpha, \beta, t)$, leads to:

$$\frac{\partial B}{\partial t} = \mu_{rev} \frac{\partial H}{\partial t} + k_1(H(t), H_{past}(t)) \cdot H - k_2(H(t), H_{past}(t)), \quad t > 0 \quad (2.17)$$

with

$$k_1(H(t), H_{past}(t)) = \frac{k_d}{2} \int_{D_1(t)} P(\alpha, \beta) d\alpha d\beta + \frac{k_d}{2} \int_{D_2(t)} P(\alpha, \beta) d\alpha d\beta \quad (2.18)$$

and

$$k_2(H(t), H_{past}(t)) = \frac{k_d}{2} \int_{D_1(t)} \alpha P(\alpha, \beta) d\alpha d\beta + \frac{k_d}{2} \int_{D_2(t)} \beta P(\alpha, \beta) d\alpha d\beta. \quad (2.19)$$

Herein μ_{rev} is the reversible differential permeability. D_1 and D_2 are the domains in the Preisach plane that represent dipoles in an intermediate state, switching to positive and negative saturation, respectively. Of course, the time dependency of D_1 and D_2 is through the magnetic field $H(t)$ and its history $H_{past}(t)$.

2.3 Combined magnetodynamic model - hysteresis model

In the CPM-case, combining (2.16) and (2.5) we get

$$\frac{1}{\sigma} \frac{\partial^2 H}{\partial x^2} = \mu_d(H(x, t), H_{past}(x, t)) \frac{\partial H}{\partial t}, \quad 0 < x < d, \quad t > 0, \quad (2.20)$$

where now μ_d also depends on the space variable, through $H(x, t)$ and $H_{past}(x, t)$.

Similarly, in the RPM-case, we arrive at

$$\frac{1}{\sigma} \frac{\partial^2 H}{\partial x^2} = \mu_{rev} \frac{\partial H}{\partial t} + k_1(H(x, t), H_{past}(x, t))H - k_2(H(x, t), H_{past}(x, t)), \quad (2.21)$$

$$0 < x < d, \quad t > 0,$$

where the functions k_1 and k_2 have a similar form as (2.18) and (2.19) respectively, however now showing the x -dependency too.

As stated above, to these respective governing DEs for $H(x, t)$, we add the BCs (2.6). Finally, the IC will be taken to be

$$H(x, t = 0) = 0, \quad \begin{cases} \eta(x, \alpha, \beta, t = 0) = +1 & \text{when } \alpha + \beta < 0 \\ \eta(x, \alpha, \beta, t = 0) = -1 & \text{when } \alpha + \beta > 0 \end{cases}, \quad (2.22)$$

reflecting the chosen initial state of the material at $t = 0$. This initial state corresponds to the state reached after a sufficiently long time during which a magnetic field is enforced of the type

$$H(t) = H_m e^{-\epsilon t} \cos(2\pi f t), \quad (\text{f: frequency}) \quad (2.23)$$

where H_m is defined by (2.13) and $0 < \epsilon \ll 1$. By definition, that limit state is the 'demagnetized' state of the material. According to the Preisach model, in that state, the magnetisation of each dipole is precisely given by (2.22).

2.4 Variational formulation

Case of CPM

We proceed as in Sections 1.1-1.2. Explicitly, let $W_2^1(]0, d[)$ be the usual first order Sobolev space on the interval $]0, d[$. Multiplying both sides of (2.20) with an arbitrary test function $w \in W_2^1(]0, d[)$, integrating over the interval $]0, d[$, invoking the formula of partial integration in Sobolev spaces, (1.4), and applying the BCs (2.6), we arrive at the following variational problem:

Find the function $H(x, t)$, which for each $t > 0$ fulfills $H(\cdot, t) \in W_2^1(]0, d[)$, with $\frac{\partial H(\cdot, t)}{\partial t} \in L_2(]0, d[)$, and which moreover obeys

$$\begin{aligned} \frac{1}{\sigma} \int_0^d \frac{\partial H(x, t)}{\partial x} \frac{dw(x)}{dx} dx + \int_0^d \mu_d \frac{\partial H(x, t)}{\partial t} w(x) dx &= \frac{w(d)}{2} \frac{d\phi}{dt}, \\ \forall w \in W_2^1(]0, d[), \forall t > 0 \end{aligned} \quad (2.24)$$

along with the IC (2.22).

This variational problem may be shown to be formally equivalent with the original BVP (2.20)-(2.6)-(2.22).

Case of RPM

Proceeding similarly for (2.21), the variational equation now reads

$$\begin{aligned} \frac{1}{\sigma} \int_0^d \frac{\partial H(x, t)}{\partial x} \frac{dw(x)}{dx} dx + \int_0^d \mu_{rev} \frac{\partial H(x, t)}{\partial t} w(x) dx + \int_0^d k_1(x, t) H(x, t) w(x) dx \\ = \int_0^d k_2(x, t) w(x) dx + \frac{w(d)}{2} \frac{d\phi}{dt}, \quad \forall w \in W_2^1(]0, d[), \quad \forall t > 0. \end{aligned} \quad (2.25)$$

Here, for brevity, we denoted $k_1(x, t) = k_1(H(x, t), H_{past}(x, t))$ and similarly for $k_2(x, t)$.

2.5 Finite Element Approximation

We apply the method described in Section 1.1. Consider the $2n+1$ equidistant nodes $0 \equiv x_1 < x_2 < \dots < x_{2n} < x_{2n+1} \equiv d$. Denote $\Omega =]0, d[$ and introduce the function space

$$\begin{aligned} W_h &= \{v \in C^0(\bar{\Omega}); v|_{[x_{2s-1}, x_{2s+1}]} \text{ is a polynomial of 2nd degree, } 1 \leq s \leq n\} \\ &\subset W_2^1(\Omega) \end{aligned} \quad (2.26)$$

Let $(\varphi_i(x))_{i=1}^{2n+1}$ be the canonical basis of W_h . Thus,

$$\varphi_i(x_j) = \delta_{ij}, \quad 1 \leq j \leq 2n+1. \quad (2.27)$$

Case of CPM

Following e.g. [4], we construct a FE-approximation of (2.24) by determining the function $H_h(x, t) \in W_2^1(\Omega)$, for $t \geq 0$,

$$H_h(x, t) = \sum_{i=1}^{2n+1} c_i(t) \varphi_i(x), \quad x \in \bar{\Omega}, \quad t \geq 0, \quad (2.28)$$

which obeys the discrete version of (2.24), viz

$$\frac{1}{\sigma} \int_0^d \frac{\partial H_h(x, t)}{\partial x} \frac{dw(x)}{dx} dx + \int_0^d \hat{\mu}_d \frac{\partial H_h(x, t)}{\partial t} w(x) dx = \frac{w(d)}{2} \frac{d\phi}{dt}, \quad \forall w \in W_h, \quad t > 0 \quad (2.29)$$

along with the IC

$$H_h(x, t = 0) = 0, \quad \begin{cases} \eta(x, \alpha, \beta, t = 0) = +1 & : \alpha + \beta < 0 \\ \eta(x, \alpha, \beta, t = 0) = -1 & : \alpha + \beta > 0 \end{cases} \quad (2.30)$$

Here, we have deliberately approximated the space dependency of the differential permeability μ_d by passing to $\hat{\mu}_d$, defined by

$$\hat{\mu}_d(x, t) = \mu_d(x_{2s}, H_h(x_{2s}, t), H_{past,h}(x_{2s}, t)), \quad x_{2s-1} \leq x \leq x_{2s+1}, \quad 1 \leq s \leq n, \quad t > 0. \quad (2.31)$$

Thus, we have discretized the space dependency of μ_d by means of the values in the element midpoints, being consistent with the finite element method and resulting in a manageable memory data.

The resulting initial value problem (IVP) for the nodal values $H_h(x_i, t) \equiv c_i(t)$, $t > 0$, reads:

Find the column matrix $[C(t)] = [c_1(t), \dots, c_{2n+1}(t)]^T$ which obeys

$$[M] \frac{d[C]}{dt} + [K][C] = [F], \quad t > 0, \quad (2.32)$$

along with

$$[C(0)] = 0, \quad \begin{cases} \eta(x_{2s}, \alpha, \beta, t = 0) = +1 & : \alpha + \beta < 0 \\ \eta(x_{2s}, \alpha, \beta, t = 0) = -1 & : \alpha + \beta > 0 \end{cases}, \quad 1 \leq s \leq n. \quad (2.33)$$

Here, the mass matrix $[M]$, the stiffness matrix $[K]$ and the force matrix $[F]$ have the form:

$$[M(t)] = [M_{ij}]_{1 \leq i, j \leq 2n+1}, \quad M_{ij} = \int_0^d \hat{\mu}_d \varphi_i \varphi_j dx, \quad (2.34)$$

$$[K(t)] = [K_{ij}]_{1 \leq i, j \leq 2n+1}, \quad K_{ij} = \frac{1}{\sigma} \int_0^d \frac{d\varphi_i}{dx} \frac{d\varphi_j}{dx} dx, \quad (2.35)$$

$$[F(t)] = [F_i]_{1 \leq i \leq 2n+1}, \quad F_i = \frac{1}{2} \frac{d\phi}{dt} \delta_{i(2n+1)}. \quad (2.36)$$

Case of RPM

Proceeding in a similar way, the IVP for $H_h(x, t) \simeq H(x, t)$ shows the same form as (2.32)-(2.33), however with the mass, stiffness and force matrix now being defined by

$$[M(t)] = [M_{ij}]_{1 \leq i, j \leq 2n+1}, \quad M_{ij} = \int_0^d \hat{\mu}_{rev} \varphi_i \varphi_j dx, \quad (2.37)$$

$$[K(t)] = [K_{ij}]_{1 \leq i, j \leq 2n+1}, \quad K_{ij} = \frac{1}{\sigma} \int_0^d \frac{d\varphi_i}{dx} \frac{d\varphi_j}{dx} dx + \int_0^d \hat{k}_1(x, t) \varphi_i(x) \varphi_j(x) dx \quad (2.38)$$

$$[F(t)] = [F_i]_{1 \leq i \leq 2n+1}, \quad F_i = \int_0^d \hat{k}_2(x, t) \varphi_i(x) dx + \frac{1}{2} \frac{d\phi}{dt} \delta_{i(2n+1)}. \quad (2.39)$$

Here, for $g=\mu_{rev}$, $g=k_1$ and $g=k_2$, we put

$$\hat{g}(x, t) = g(x_{2s}, t), \quad x_{2s-1} \leq x \leq x_{2s+1}, \quad 1 \leq s \leq n, \quad t > 0. \quad (2.40)$$

For brevity we denoted

$$\hat{k}_1(x, t) = \hat{k}_1(H_h(x, t), H_{h,past}(x, t)) \quad (2.41)$$

and similarly for $\hat{k}_2(x, t)$.

The IVP's (2.32)-(2.33), where the mass matrix, stiffness and force matrices are given by (2.34)-(2.36) in the case of the CPM and by (2.37)-(2.41) in the case of the RPM, are nonlinear. Indeed in the CPM-case the elements of $[M]$ depend on the (approximated) differential permeability $\hat{\mu}_d$ that is a function of the (approximated) magnetic field $H_h(x, t)$ and its history $H_{h,past}(x, t)$. Similarly, in the RPM-case, the elements of $[M]$ depend on $\hat{\mu}_{rev}$, that is a function of $H_h(x, t)$, while the components of the stiffness matrix and of the force matrix depend on \hat{k}_1 and \hat{k}_2 respectively, both being functions of $H_h(x, t)$ and $H_{h,past}(x, t)$.

2.6 Time discretisation: Modified Crank-Nicholson method

The nonlinear IVPs derived above will be solved numerically by a suitable FDM, viz by a modified Crank-Nicholson scheme, cf. the procedure described in Section 1.2, combined with an iterative procedure. Thus, we will properly take into account the hysteresis behaviour of the material, reflected in the dependence of μ_d on H and H_{past} in the CPM-case and reflected in the dependence of μ_{rev} on H and in the dependence of D_1 and D_2 on H and H_{past} in the RPM-case.

Case of CPM

Let Δt be a time step and let $t_l = l \cdot \Delta t$, $l = 1, 2, 3, 4, \dots$, be the corresponding equidistant time points. We want to define an approximation $H_l^*(x)$ of $H_h(x, t_l)$,

$$H_l^*(x) = \sum_{i=1}^{2n+1} c_i^{(l)} \varphi_i(x) \simeq \sum_{i=1}^{2n+1} c_i(t_l) \varphi_i(x), \quad (2.42)$$

by means of a recurrent set of nonlinear systems for

$$[C^{(l)}] = [c_1^{(l)}, c_2^{(l)}, \dots, c_{2n+1}^{(l)}]^T, l = 1, 2, \dots \quad (2.43)$$

First, notice the discontinuities with respect to time of the differential permeability $\hat{\mu}_d(x_{2s}, t) = \frac{\partial B_h}{\partial H_h}(x_{2s}, t)$, (2.31), in two cases: (a) when $\frac{dc_{2s}}{dt}$ changes sign, (b) when a minor order loop is closed, cf. Fig.2.8. From (2.32) we get

$$\int_{t_l}^{t_{l+1}} [M] \frac{d[C]}{dt} dt + [K] \int_{t_l}^{t_{l+1}} [C] dt = \int_{t_l}^{t_{l+1}} [F] dt, t > 0. \quad (2.44)$$

To properly take into account the *possible* jump of $\hat{\mu}_d(x_{2s}, t)$ in the interval $[t_l, t_{l+1}]$, we approximate the first term as

$$\int_{t_l}^{t_{l+1}} [M] \frac{d[C]}{dt} dt \simeq [\tilde{M}^{(l+1)}]([C^{(l+1)}] - [H_{ext}^{(l+1)}]) + [\tilde{M}^{(l)}]([H_{ext}^{(l+1)}] - [C^{(l)}]), \quad (2.45)$$

where $[\tilde{M}^{(l)}]$ is a square matrix and $[H_{ext}^{(l+1)}]$ is a column matrix, defined by

$$\tilde{M}_{ij}^{(l)} = \int_0^d \tilde{\mu}_d(x, t_l) \varphi_i(x) \varphi_j(x) dx, \quad i, j = 1, \dots, 2n+1, \quad (2.46)$$

$$H_{ext, 2r-1}^{(l+1)} = \frac{1}{2} [c_{2r-1}^{(l+1)} + c_{2r-1}^{(l)}], \quad r = 1, \dots, n+1, \quad (2.47)$$

$$H_{ext, 2r}^{(l+1)} = \begin{cases} \frac{1}{2} [c_{2r-1}^{(l+1)} + c_{2r-1}^{(l)}] & \text{if there is no jump of } \tilde{\mu}_d(x, t) \text{ in } [t_l, t_{l+1}] \\ g_{2r, t_l} & \text{if there is a jump of } \tilde{\mu}_d(x, t) \text{ in } [t_l, t_{l+1}] \end{cases}, \quad (2.48)$$

$r = 1, \dots, n.$

Here, g_{2r, t_l} is the approximation of the extremal value of $c_{2r}(t)$ in the interval $[t_l, t_{l+1}]$, as shown in Fig.2.8, corresponding to the cases (a) and (b) mentioned above. Moreover in (2.46), $\tilde{\mu}_d(x, t_l)$ stands for the approximation of $\hat{\mu}_d(x, t_l)$, (2.31), which is found when we use $H_p^*(x)$, $1 \leq p \leq l$, to describe the dependency on the magnetic field and its history up to $t = t_l$.

Let $0 \leq \theta \leq 1$ be a parameter of the method. We approximate the 2nd and 3rd term of (2.44) as follows

$$[K] \int_{t_l}^{t_{l+1}} [C] dt \simeq [K] (\theta [C^{(l+1)}] + (1 - \theta) [C^{(l)}]) \Delta t, \quad (2.49)$$

$$\int_{t_l}^{t_{l+1}} [F] dt \simeq (\theta [F(t_{l+1})] + (1 - \theta) [F(t_l)]) \Delta t. \quad (2.50)$$

Finally, combining (2.45), (2.49) and (2.50), we get from (2.44)

$$\begin{aligned} & \left(\frac{[\tilde{M}^{(l+1)}]}{\Delta t} + \theta [K] \right) [C^{(l+1)}] = \left(\frac{[\tilde{M}^{(l)}]}{\Delta t} - (1 - \theta) [K] \right) [C^{(l)}] \\ & + \left(\frac{[\tilde{M}^{(l+1)}] - [\tilde{M}^{(l)}]}{\Delta t} \right) [H_{ext}^{(l+1)}] + \theta ([F(t_{l+1})] + (1 - \theta) [F(t_l)]), \quad l = 0, 1, 2, \dots, \end{aligned} \quad (2.51)$$

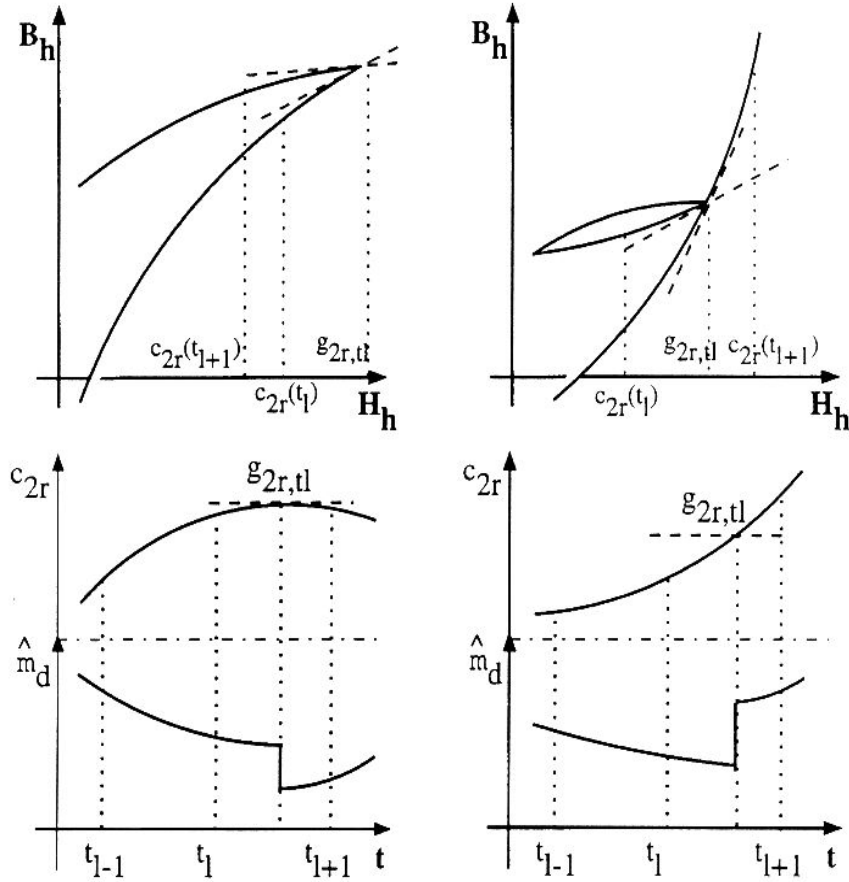


Figure 2.8: *Parabolic interpolation arc for the magnetic field (upper curve); corresponding differential permeability (lower curve)*

along with

$$[C^{(0)}] = 0. \quad (2.52)$$

As the matrix $[\tilde{M}^{(l+1)}]$ and the matrix $[H_{ext}^{(l+1)}]$, introduced in (2.46) and (2.47)-(2.48), depend on the unknown $H_{l+1}^*(x)$, we set up a Newton-Raphson iteration procedure to solve the nonlinear system (2.51) at each time point $t = t_l$. The approximation of $C^{(l)}$ at the k -th iteration level is denoted by $C^{(l),(k)}$. The corresponding approximation of (2.28) is written as $H_h^{(l),(k)}(x)$. In the final iteration level n_l we write $H_h^{(l)} := H_h^{(l),(n_l)}$, which is then used as the input for the iteration procedure at the subsequent time point t_{l+1} .

In practice, convergence has been observed in 4 iterations.

Case of RPM

Let again $0 \leq \theta \leq 1$ be a parameter of the method. We now define an approximation $H_l^*(x)$ of $H_h(x, t_l)$, (2.42), by means of the following recurrent set of nonlinear

systems for $[C^{(l)}]$, (2.43), $l = 1, 2, \dots$,

$$\begin{aligned} \left(\frac{[\tilde{M}^{(l+1)}]}{\Delta t} + \theta[\tilde{K}^{(l+1)}] \right) [C^{(l+1)}] &= \left(\frac{[\tilde{M}^{(l+1)}]}{\Delta t} - (1 - \theta)[\tilde{K}^{(l)}] \right) [C^{(l)}] \\ &+ \theta[\tilde{F}^{(l+1)}] + (1 - \theta)[\tilde{F}^{(l)}], \quad l = 0, 1, 2, \dots, \end{aligned} \quad (2.53)$$

along with

$$[C^{(0)}] = 0. \quad (2.54)$$

Here, the approximated mass matrix $[\tilde{M}^{(l)}] \simeq [M(t_l)]$, stiffness matrix $[\tilde{K}^{(l)}] \simeq [K(t_l)]$ and force matrix $[\tilde{F}^{(l)}] \simeq [F(t_l)]$ are defined by

$$\tilde{M}_{ij}^{(l)} = \int_0^d \tilde{\mu}_{rev}^{(l)} \varphi_i \varphi_j dx, \quad (2.55)$$

$$\tilde{K}_{ij}^{(l)} = \frac{1}{\sigma} \int_0^d \frac{d\varphi_i}{dx} \frac{d\varphi_j}{dx} dx + \int_0^d \tilde{k}_1^{(l)}(x) \varphi_i(x) \varphi_j(x) dx, \quad (2.56)$$

$$\tilde{F}_j^{(l)} = \int_0^d \tilde{k}_2^{(l)}(x) \varphi_j(x) dx + \frac{1}{2} \frac{d\phi}{dt} \delta_{j(2n+1)}, \quad (2.57)$$

with

$$\tilde{\mu}_{rev}^{(l)} = (1 - \theta) \hat{\mu}_{rev}(H_{l-1}^*(x)) + \theta \hat{\mu}_{rev}(H_l^*(x)). \quad (2.58)$$

Moreover, $\tilde{k}_1^{(l)}(x)$, appearing in (2.56), is the approximation of $\hat{k}_1(x, t_l)$, (2.41), that is found when we use $H_p^*(x)$, $1 \leq p \leq l$, to describe the dependency on the magnetic field and its history up to $t = t_l$; $\tilde{k}_2^{(l)}(x)$ is obtained in a similar way.

As the mass, stiffness and force matrices, entering (2.53), all depend on the unknown, as just mentioned, we again set up a usual Newton-Raphson iterative procedure to solve the nonlinear system (2.53) at every time point t_l . Again, in practice, convergence has been observed for 4 iterations.

2.7 Experimental Validation

The magnetodynamic model, including either the CPM or the RPM, as well as its FE - FD discretisation, as outlined in this chapter, has been verified by numerous experiments. The numerical results obtained for relevant physical quantities, such as the BH -loops and the iron losses, are in good agreement with the values obtained by measurements.

Here, we consider two materials with different magnetic structure, referred to as Mat.1 and Mat.2. The former is a material with high carbide contents and large mechanical stresses. Mat.2, known as V-450-50-E in the classification of [8], results from Mat.1 by the process of decarbonizing and stress relieving. We compare the quasi-static and the dynamic behaviour of the two materials.

The quasi-static behaviour is obtained at sufficiently slowly varying period magnetic fields, such that a BH -loop occurs in which dynamic effects can be neglected. Typically we can take 10 seconds for one period.

A. Quasi-static characterisation

Fig.2.9 shows the measured Preisach functions $P(\alpha, \beta)$, being introduced in Section 2.2.2. for Mat.1 and Mat.2. The Preisach function is measured by the technique of [9], which is based upon the Everett theory. Notice that the Preisach function for Mat.1 shows two extrema, while Mat.2 shows only one extremum. As a test for these Preisach functions, Fig.2.10 and Fig.2.11 show a very good agreement between the quasi-static measured BH -loops and the loops obtained from the hysteresis model.

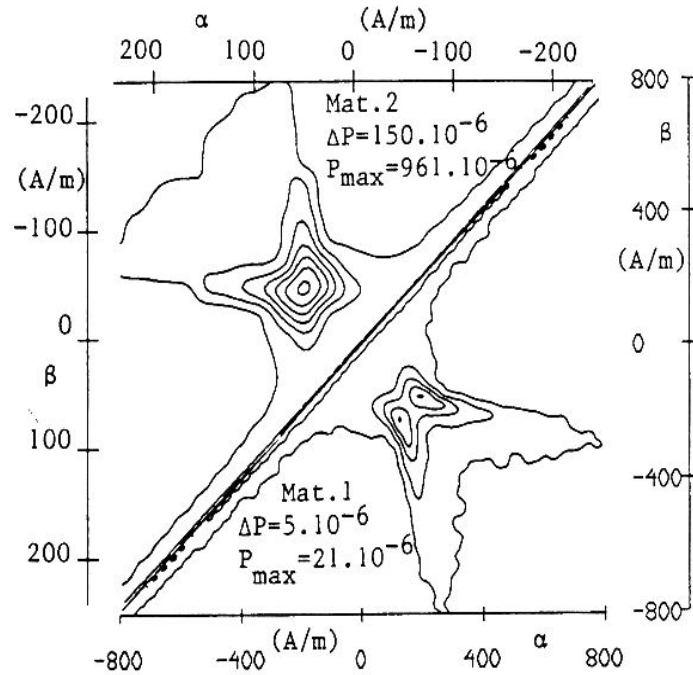


Figure 2.9: Preisach function $P(\alpha, \beta)$ for Mat.1 and Mat.2, ΔP denoting the difference between 2 neighbouring isolines of the Preisach function. The most inner isoline is the one with the highest P -value, denoted by P_{max}

B. Dynamic characterisation

We now consider the following type of excitation: we enforce the time dependent magnetic field strength at the outer boundary of the lamination, denoted by $H_b(t)$. The average magnetic induction $B_a(t)$ through the lamination is a direct result. The calculated and the measured dynamic $B_a H_b$ -loops are observed to coincide, which, of course, results in a striking good agreement between the numerically obtained and the measured values of the total iron losses. The numerical values are evaluated from the expression (2.8).

The electrical conductivity σ , entering (2.20)-(2.21), is directly measured. It takes the values $\sigma = 29.2 \cdot 10^5$ and $\sigma = 30.7 \cdot 10^5$ for Mat.1 and Mat.2 respectively. The parameter θ in Section 2.6 is given the value 0.5.

B.1 Limit cycles

The enforced magnetic field $H_b(t)$ is taken to be a piecewise linear function of time, namely the piecewise linear interpolant of the extremal values $H_b(t_i)$ in the successive points $t_i, i=0,1,2,\dots$

For brevity we denote this as:

$$\begin{bmatrix} H_b(t) \\ t \end{bmatrix} = \begin{bmatrix} 0 & H_b(t_1) & H_b(t_2) & \dots & H_b(t_i) & H_b(t_{i+1}) & \dots \\ 0 & t_1 & t_2 & \dots & t_i & t_{i+1} & \dots \end{bmatrix}.$$

Mat.1

For this material the CPM is found to be sufficiently accurate for describing the dynamic behaviour. Fig.2.12 shows the $B_a H_b$ -loops, corresponding to the field

$$\begin{bmatrix} H_b(t) \\ t \end{bmatrix} = \begin{bmatrix} 0 & 1200 & -1200 & 1200 & -1200 & \dots \\ 0 & \frac{1}{4f} & \frac{3}{4f} & \frac{5}{4f} & \frac{7}{4f} & \dots \end{bmatrix}, \quad f = 500Hz,$$

while Fig.2.14 gives the total iron losses for one cycle as a function of the frequency f .

Mat.2

The hysteresis behaviour of this second material can no longer be described adequately by the CPM. Instead, this behaviour turns out to be rate-dependent. However, it can be modelled correctly by the RPM, with $k = 55m/As$. (Moreover, this value itself is observed to be frequency independent). Fig.2.13 and Fig.2.14 show the $B_a H_b$ -loops and the corresponding total iron losses respectively; the measured values are compared with the numerical values (obtained by both using the RPM and the CPM). In this case the enforced excitation reads

$$\begin{bmatrix} H_b(t) \\ t \end{bmatrix} = \begin{bmatrix} 0 & 400 & -400 & 400 & -400 & \dots \\ 0 & \frac{1}{4f} & \frac{3}{4f} & \frac{5}{4f} & \frac{7}{4f} & \dots \end{bmatrix}, \quad f = 500Hz.$$

For the FEM we typically take $n=10$ (quadratic) elements. In the time discretisation we observed that the time step Δt must be taken much smaller in the RPM-case than in the CPM to retain the same accuracy, typically $\Delta t = \frac{1}{4000f}$ and $\Delta t = \frac{1}{400f}$ respectively. The parameter θ in Section 2.6 is given the value 0.5.

B.2 Minor Loops

The mathematical model outlined in this chapter also provides adequate results for the minor order loops $B_a H_b$, corresponding to the *local* extrema of the magnetic field $H(t)$, as described for instance in [10]. Again for Mat.1 the dynamic behaviour is found to be accurately modelled when using the CPM, while for Mat.2 the RPM must be used to describe the hysteresis behaviour properly. As an example, we consider the $B_a H_b$ -loops for Mat.1 and Mat.2 in the case of H-excitation, under the enforced fields

$$\begin{bmatrix} H_b(t) \\ t \end{bmatrix} = \begin{bmatrix} 0 & -400 & 400 & -150 & 200 & -150 & 200 & -150 & 200 & -400 & 0 \\ 0 & 0.02 & 0.03 & 0.0368 & 0.0412 & 0.0455 & 0.0498 & 0.0542 & 0.0585 & 0.0660 & 0.071 \end{bmatrix}$$

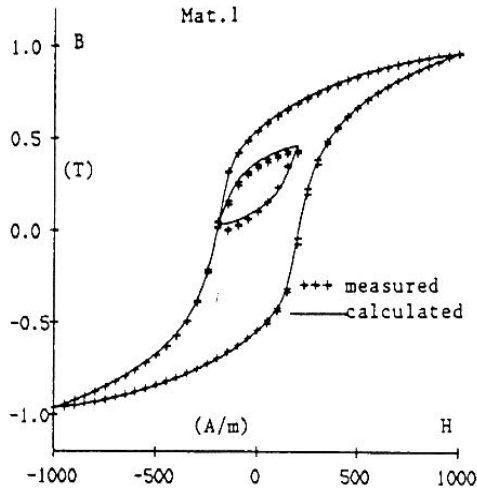


Figure 2.10: *Quasi static B-H loop for Mat.1*

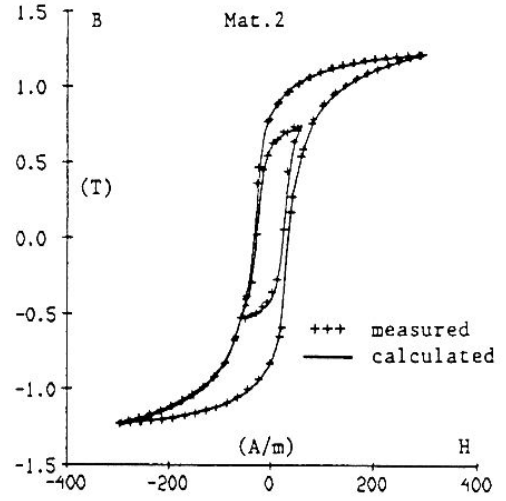


Figure 2.11: *Quasi static B-H loop for Mat.2*

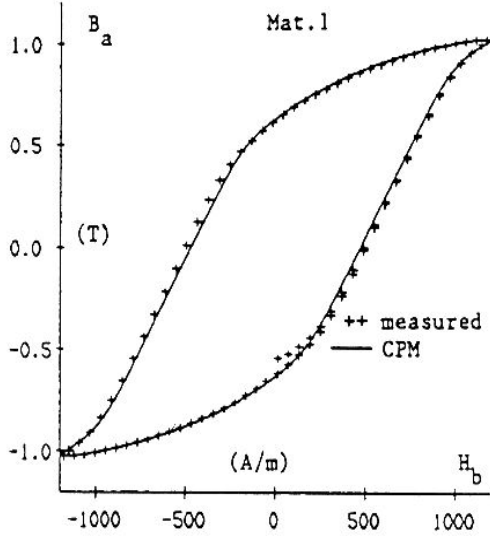


Figure 2.12: *B_aH_b-loop for Mat.1 with H-excitation*

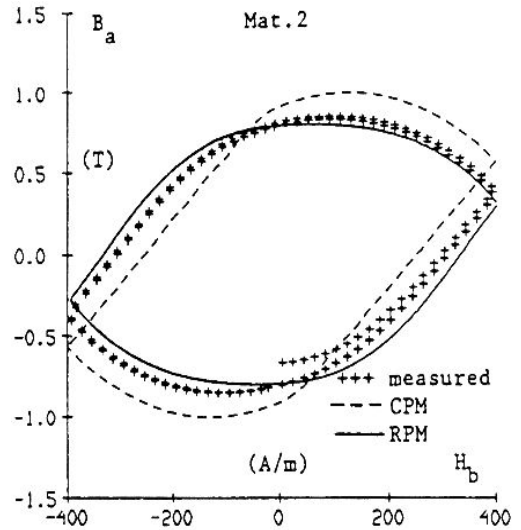


Figure 2.13: *B_aH_b-loop for Mat.2 with H-excitation*

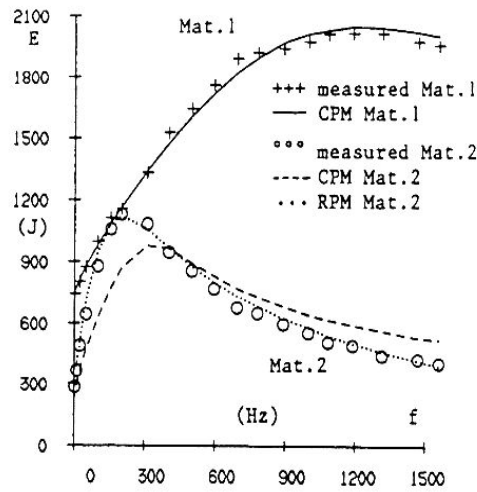


Figure 2.14: Total electromagnetic losses, H -excitation

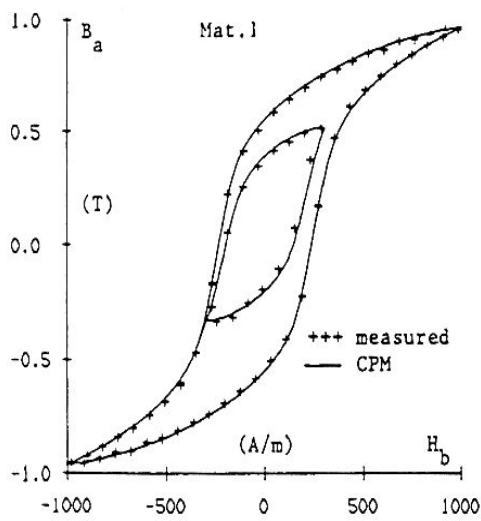


Figure 2.15: $B_a H_b$ -loop for Mat.1 with minor loops

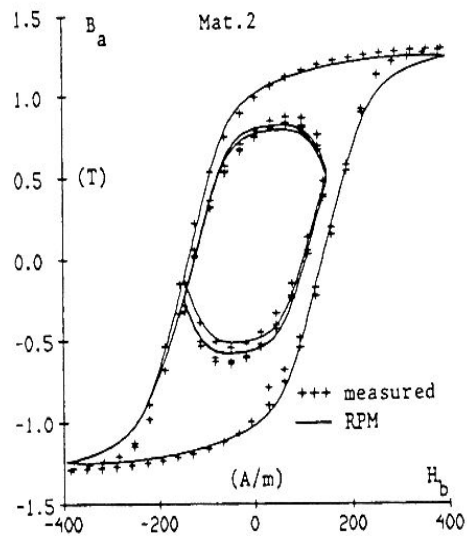


Figure 2.16: $B_a H_b$ -loop for Mat.2 with minor loops

and

$$\begin{bmatrix} H_b(t) \\ t \end{bmatrix} = \begin{bmatrix} 0 & 1000 & -1000 & 1000 & -300 & 300 & -1000 \\ 0 & 0.01 & 0.03 & 0.05 & 0.063 & 0.069 & 0.082 \end{bmatrix}$$

respectively. Fig.2.15 and Fig.2.16 show a good agreement between the measured and the numerically obtained loops.

3 2D Nonlinear Parabolic Problems with a scalar hysteresis model

3.1 A motivating physical problem and its mathematical model

In this part we deal with 2D nonlinear parabolic problems with memory effects arising in the context of electromagnetic field calculations in one lamination of an electrical machine. These field computations are important for the evaluation of the electromagnetic loss in the magnetic circuit. A part of such a magnetic circuit is shown in Fig.3.1.

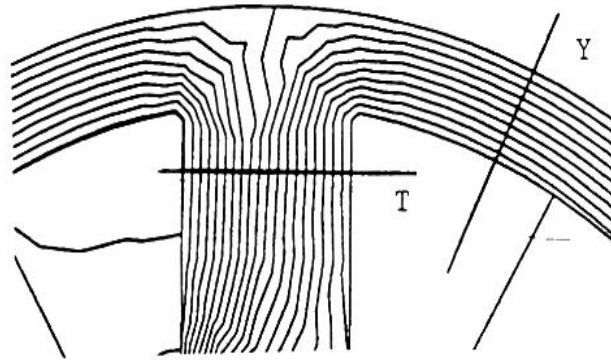


Figure 3.1: *A part of the magnetic circuit, with corresponding flux lines; T:tooth, Y:yoke*

Fig.3.2-3.3 show the cross section of a tooth and a yoke respectively. The electromagnetic losses are determined from the magnetic field \bar{H} in a cross section S , both of the tooth and the yoke, orthogonal to the direction of the time varying, enforced flux $\phi(t)$.

The relevant Maxwell equations for the magnetic field \bar{H} , the electric field \bar{E} , the electric flux density \bar{D} and the magnetic induction \bar{B} are given by (1.43)-(1.45), while the constitutive relation for the current density vector \bar{J} is given by (1.50). Again neglecting the displacement current and the electric charge density, the magnetic field \bar{H} is found to be related to the magnetic induction \bar{B} by the following DE:

$$-\text{rot}(\text{rot}(\bar{H})) = \sigma \frac{\partial \bar{B}}{\partial t} \quad \text{in } S, \quad t > 0. \quad (3.1)$$

Integrating both sides over the section S , using Green's formula, see (1.21), and invoking the definition of the total flux, viz

$$\phi(t) = \int_S \bar{B} \cdot d\bar{S}, \quad t > 0, \quad (3.2)$$

\bar{H} is seen to obey the following nonlocal, inhomogenous BC on ∂S :

$$\int_{\partial S} \text{rot} \bar{H} \cdot d\bar{l} = -\sigma \frac{d\phi(t)}{dt}, \quad t > 0. \quad (3.3)$$

The magnetic motoric force per unit interval of the space variable in the flux direction (with unit-vector $\bar{1}_{fl}$) may be assumed to be space independent along ∂S , as the magnetic flux lines, shown in Fig.3.1, can be approximated to be uniform along ∂S , see [11]. Thus, denoting the corresponding segment along a flux line by Γ , the following inhomogeneous Dirichlet BC must be imposed:

$$\int_{\Gamma} \bar{H} \cdot \bar{1}_{fl} d\gamma = C_b(t), \quad (3.4)$$

Here $C_b(t)$, which varies in time, but which is space independent along ∂S , is *not* known a priori, but must be determined as part of the problem.

Finally, the system (3.1)-(3.4) must be completed with initial data, viz

$$\bar{H} = 0, \quad \begin{cases} \eta(\alpha, \beta, t) = +1 & \text{when } \alpha + \beta < 0 \\ \eta(\alpha, \beta, t) = -1 & \text{when } \alpha + \beta > 0 \end{cases}, \quad \text{in } S, \text{ at } t = 0, \quad (3.5)$$

corresponding to the demagnetized state of the material.

Actually, the value $C_b(t)$ is the physical relevant quantity in the present field problem. Indeed, the electromagnetic loss [joule] over a time interval (T_1, T_2) per unit interval of the space variable in the flux direction is given by [5]:

$$E = \int_{T_1}^{T_2} C_b(t) \frac{d\phi}{dt} dt. \quad (3.6)$$

Assuming the material isotropic, \bar{H} may taken to be unidirectional, i.e. $\bar{H} = H \cdot \bar{1}_{fl}$. Consequently, also \bar{B} is unidirectional. Therefore, a *scalar* hysteresis model may be used to describe the BH -relation. We again will use the CPM and RPM presented in the previous sections. Thus, we are left with a scalar parabolic problem for H , with a *nonlocal* Neumann boundary condition on ∂S , as well as with a Dirichlet side condition, in which the boundary value of H on ∂S is unknown too.

Alternatively, we can consider the parabolic problem where the function $C_b(t)$, entering (3.4), is given, while the flux $\phi(t)$, appearing in (3.3), must be sought as part of the problem. We will consider the parabolic problem in both the tooth and the yoke cross section, cf. Fig.3.2 and Fig.3.3, where we use a cartesian and a cylindrical coordinate system, respectively.

3.2 Combined magnetodynamic-hysteresis model

3.2.1 Parabolic problem in a tooth cross-section S

Case of CPM

Taking the cartesian coordinate system as in Fig.3.2, the problem (3.1)-(3.5) for the magnetic field $\vec{H} = H \cdot \bar{1}_{fl}$, ($\bar{1}_{fl} = \bar{1}_z$), in a cross section S of a tooth simplifies to the following scalar parabolic problem for $H(x, y, t)$:

$$\frac{1}{\sigma} \left(\frac{\partial^2 H}{\partial x^2} + \frac{\partial^2 H}{\partial y^2} \right) = \mu_d(H(x, y, t), H_{past}(x, y, t)) \frac{\partial H}{\partial t} \quad \text{in } S, \quad t > 0, \quad (3.7)$$

$$\int_{\partial S} \frac{\partial H}{\partial n} dl = \sigma \frac{d\phi(t)}{dt}, \quad t > 0, \quad (3.8)$$

$$H = C_b(t), \quad \text{on } \partial S, \quad t > 0, \quad (3.9)$$

$$H = 0, \quad \begin{cases} \eta(x, y, \alpha, \beta, t) = +1 & \text{when } \alpha + \beta < 0 \\ \eta(x, y, \alpha, \beta, t) = -1 & \text{when } \alpha + \beta > 0 \end{cases}, \quad \forall (x, y) \in S, \quad \text{at } t = 0. \quad (3.10)$$

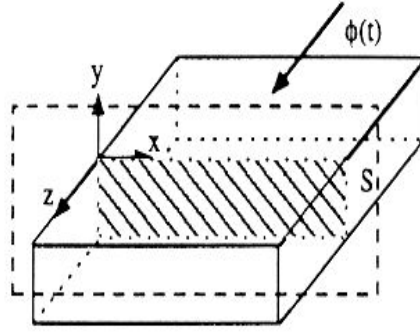


Figure 3.2: Cross section of a tooth, orthogonal to the flux line

Case of RPM

Now the governing DE becomes

$$\frac{1}{\sigma} \left(\frac{\partial^2 H}{\partial x^2} + \frac{\partial^2 H}{\partial y^2} \right) = \mu_{rev} \frac{\partial H}{\partial t} + k_1(H(x, y, t), H_{past}(x, y, t))H - k_2(H(x, y, t), H_{past}(x, y, t)) \quad \text{in } S, \quad t > 0, \quad (3.11)$$

along with the BCs (3.8)-(3.9) and the IC (3.10).

In both cases, as said above, we have one of the two situations: either $C_b(t)$ is not given a priori, while $\phi(t)$ is given (enforced), or vice versa.

3.2.2 Parabolic problem in a yoke cross section S

Case of CPM

Taking the cylindrical coordinate system as in Fig.3.3, the problem (3.1)-(3.5) for the magnetic field $\vec{H} = H\vec{1}_{fl}$, ($\vec{1}_{fl} = \vec{1}_\varphi$), in a cross section S of a yoke can now be reduced to the following scalar parabolic problem for $H(r, z; t)$:

$$\frac{1}{\sigma} \left(\frac{\partial}{\partial r} \left(\frac{1}{r} \frac{\partial}{\partial r} (rH) \right) + \frac{\partial^2 H}{\partial z^2} \right) = \mu_d(H(r, z, t), H_{past}(r, z, t)) \frac{\partial H}{\partial t},$$

$$\text{in } S, \quad t > 0, \quad (3.12)$$

$$\int_{\partial S} \left[\frac{\partial H}{\partial z} n_z + \frac{1}{r} \frac{\partial (rH)}{\partial r} n_r \right] dl = \sigma \frac{d\phi(t)}{dt}, \quad t > 0, \quad (3.13)$$

$$rH = C_b(t), \quad \text{on } \partial S, \quad t > 0, \quad (3.14)$$

$$H = 0, \quad \begin{cases} \eta(r, z, \alpha, \beta, t) = +1 & \text{when } \alpha + \beta < 0 \\ \eta(r, z, \alpha, \beta, t) = -1 & \text{when } \alpha + \beta > 0 \end{cases}, \quad \forall (r, z) \in S, \quad \text{at } t = 0. \quad (3.15)$$

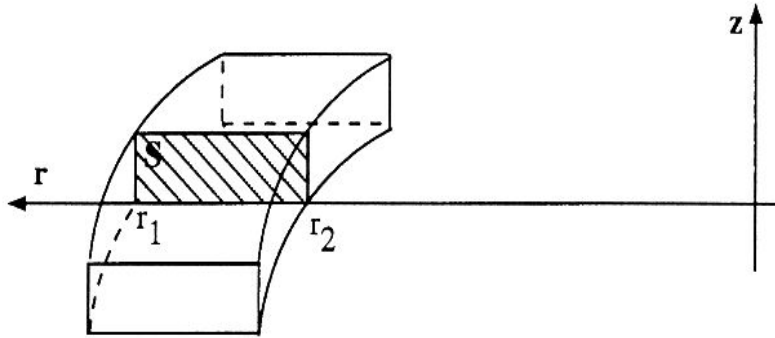


Figure 3.3: Cross section of a yoke, orthogonal to the flux line

Case of RPM

Now the governing DE becomes

$$\frac{1}{\sigma} \left(\frac{\partial}{\partial r} \left(\frac{1}{r} \frac{\partial}{\partial r} (rH) \right) + \frac{\partial^2 H}{\partial z^2} \right) = \mu_{rev} \frac{\partial H}{\partial t} + k_1(H(r, z, t), H_{past}(r, z, t))H$$

$$- k_2(H(r, z, t), H_{past}(r, z, t)) \quad \text{in } S, \quad t > 0, \quad (3.16)$$

where we retain the BCs (3.13)-(3.14) and the IC (3.15).

In both cases, a similar remark concerning $C_b(t)$ and $\phi(t)$ applies as in Section 3.2.1.

3.3 Variational formulation

3.3.1 Parabolic problem in a tooth cross-section S

Case of CPM

To derive a suitable variational form of this problem, we introduce the function space

$$V = \{v \in W_2^1(S) \mid v|_{\partial S} \text{ is constant}\}. \quad (3.17)$$

Here $W_2^1(S)$ is the usual first order Sobolev space on S and the condition " $v|_{\partial S}$ is constant " must be understood in the sense of traces, as defined e.g. in [2].

Then, multiplying both sides of (3.7) with a test function $v \in V$, integrating over S , applying Green's formula (1.21) and invoking the boundary condition (3.8), the problem (3.7)-(3.10) is found to be (formally) equivalent with the following variational problem:

Find $H(x, y; t)$, obeying $H \in V$ and $\frac{\partial H}{\partial t} \in L_2(S)$ for every $t > 0$, such that

$$\int_S \mu_d \frac{\partial H}{\partial t} v \, dx dy + \frac{1}{\sigma} \int_S \text{grad} H \cdot \text{grad} v \, dx dy = \frac{d\phi(t)}{dt} v|_{\partial S}, \forall v \in V, t > 0 \quad (3.18)$$

along with the IC (3.10)

Notice that by the requirement $H \in V$ for every $t > 0$, (3.9) is automatically taken into account.

Case of RPM

The variational form of the problem (3.11), (3.8)-(3.10), is obtained in a similar way:

Find $H(x, y; t)$, obeying $H \in V$ and $\frac{\partial H}{\partial t} \in L_2(S)$ for every $t > 0$, such that

$$\begin{aligned} \int_S \mu_{rev} \frac{\partial H}{\partial t} v \, dx dy + \frac{1}{\sigma} \int_S \text{grad} H \cdot \text{grad} v \, dx dy + \int_S k_1(x, y, t) H v \, dx dy \\ = \int_S k_2(x, y, t) v \, dx dy + \frac{d\phi(t)}{dt} v|_{\partial S}, \forall v \in V, t > 0, \end{aligned} \quad (3.19)$$

along with the IC (3.10).

3.3.2 Parabolic problem in a yoke cross section S

Case of CPM

Introducing the new unknown $\hat{H}(r, z; t) = rH(r, z; t)$ and retaining the function space V , (3.17), the problem (3.12)-(3.15) may be reduced to the (formally) equivalent variational problem:

Find $\hat{H}(r, z; t)$, obeying $\hat{H} \in V$ and $\frac{\partial \hat{H}}{\partial t} \in L_2(S)$ for every $t > 0$, such that

$$\int_S \mu_d \frac{1}{r} \frac{\partial \hat{H}}{\partial t} v \, dr dz + \frac{1}{\sigma} \int_S \frac{1}{r} \text{grad} \hat{H} \text{grad} v \, dr dz = \frac{d\phi(t)}{dt} v|_{\partial S}, \forall v \in V, t > 0, \quad (3.20)$$

along with the IC (3.15), rewritten for \hat{H} .

Case of RPM

The problem (3.16), (3.13)-(3.15), now leads to the following variational problem:

Find $\hat{H}(r, z; t)$, obeying $\hat{H} \in V$ and $\frac{\partial \hat{H}}{\partial t} \in L_2(S)$ for every $t > 0$, such that

$$\begin{aligned} \int_S \mu_{rev} \frac{1}{r} \frac{\partial \hat{H}}{\partial t} v \, dr dz + \frac{1}{\sigma} \int_S \frac{1}{r} \text{grad} \hat{H} \cdot \text{grad} v \, dr dz + \int_S \frac{1}{r} k_1(r, z, t) \hat{H} v \, dr dz \\ = \int_S k_2(r, z, t) v \, dr dz + \frac{d\phi(t)}{dt} v|_{\partial S}, \quad \text{for every } v \in V, t > 0, \end{aligned} \quad (3.21)$$

along with the IC (3.15), rewritten for \hat{H} .

Notice that, by the choice of the new unknown \hat{H} , we arrive at a variational equation similar to (3.18) and (3.19), respectively, apart from a weight factor $\frac{1}{r}$, (which is of course smooth in S), entering the integrands. This is particularly attractive from computational point of view, viz when constructing the mass and stiffness matrices in the FEM-FDM, outlined in the next section, starting from the variational problems.

3.4 Nonstandard FE-approximation in the space variable

We extend the method described in Section 1.1, to take into account the nonstandard BCs.

3.4.1 Field problem in a tooth cross section S

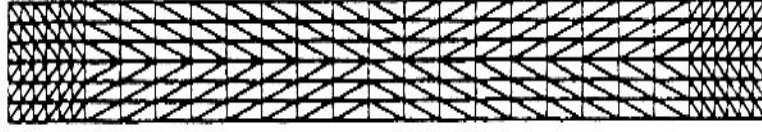
For the triangulation τ_h (h mesh parameter), shown in Fig.3.4, we consider a usual quadratic finite element mesh (with n_T the number of triangles).

By $\varphi_j(x, y)$, ($j = 1, \dots, J$), we denote the *standard cardinal* basis functions, associated to the nodes (x_j, y_j) , ($j = 1, \dots, J$), J being the total number of nodes. Here, the nodes, being either vertices of the triangles or midpoints of their sides, are numbered such that the first I of them, $I < J$, belong to the open domain S . We then have, with $C^0(\bar{S})$ being the space of continuous functions on \bar{S} and with $P_2(T)$ being the space of polynomials of degree ≤ 2 on the triangle T ,

$$X_h \equiv \left\{ v \in C^0(\bar{S}); v|_T \in P_2(T), \forall T \in \tau_h \right\} = \text{span}(\varphi_j)_{j=1}^J \quad (3.22)$$

and

$$X_{0h} \equiv \left\{ v \in X_h; v = 0 \text{ on } \partial S \right\} = \text{span}(\varphi_j)_{j=1}^I \quad (3.23)$$

Figure 3.4: The triangulation τ_h of S

Next we introduce the special function

$$\psi_{I+1}(x, y) = \sum_{j=I+1}^J \varphi_j(x, y) \in X_h \quad (3.24)$$

On a side ζ of $T \in \tau_h$, for which $\zeta \subset \partial S$, we have $\psi_{I+1}|_{\zeta} \equiv 1$, as clearly $\psi_{I+1}|_{\zeta}$ is a quadratic function of one variable (either x or y) showing the value 1 in the 3 nodes on ζ . Consequently,

$$\psi_{I+1} \equiv 1 \text{ on } \partial S \quad (3.25)$$

Moreover, ψ_{I+1} is readily understood to vanish throughout S apart from the triangles $T \in \tau_h$ adjacent to ∂S .

Writing, for convenience, $\psi_j = \varphi_j$, $1 \leq j \leq I$, we finally define

$$V_h = \text{span}(\psi_j)_{j=1}^{I+1} = X_{0h} \oplus \text{span}(\psi_{I+1}). \quad (3.26)$$

This space V_h is suitable for a conforming FEM as

$$V_h \subset V. \quad (3.27)$$

Indeed, for $v \in V_h$ one evidently has $v \in X_h \subset W_2^1(S)$, while also v is constant on ∂S , due to (3.25). Moreover, the particular choice of ψ_{I+1} , (3.24), will turn out to be attractive from computational point of view.

From here on we must distinguish between the cases CPM and RPM.

Case of CPM

The finite element approximation $H_h(x, y; t) \in V_h$ of $H(x, y; t)$ is defined by a variational problem similar to (3.18), (3.10), now with V replaced by V_h . Here, we simplify the space dependency of μ_d , by passing to $\hat{\mu}_d \simeq \mu_d$,

$$\begin{aligned} & \hat{\mu}_d(x, y, t, H_h(x, y; t), H_{h,past}(x, y; t)) \\ &= \mu_d(x_T^c, y_T^c, t, H_h(x_T^c, y_T^c, t), H_{h,past}(x_T^c, y_T^c, t)), \text{ in } T, \forall T \in \tau_h, t > 0 \end{aligned} \quad (3.28)$$

where (x_T^c, y_T^c) is the center of gravity of T . This will allow us to take properly into account the non-linear and hysteresis effects, resulting in the complicated form of

the differential permeability μ_d . μ_d now depends upon the finite element approximation $H_h(x, y; t)$ and $H_{h,past}(x, y; t)$ of the magnetic field $H(x, y; t)$ and its history $H_{past}(x, y; t)$ respectively.

Explicitly, decomposing H_h as

$$H_h(x, y; t) = \sum_{j=1}^{I+1} c_j(t) \psi_j(x, y), \quad t > 0, \quad (3.29)$$

we have $c_j(t) = H_h(x_j, y_j; t)$, $1 \leq j \leq I$, and $c_{I+1}(t) = H_h(x, y; t)|_{\partial S}$, due to the proper choice of the basis functions of V_h , (3.26). A similar result holds for the finite element approximation $H_{h,past}(x, y; t)$ of $H_{past}(x, y; t)$, the expansion coefficients now being denoted as $c_{past,1}(t), c_{past,2}(t), \dots, c_{past,I+1}(t)$.

Thus, we are led to a system of first order ODEs for the coefficient functions $c_j(t)$, $1 \leq j \leq I + 1$, viz,

$$[M(t)] \frac{d[C]}{dt} + [K][C] = [F], \quad t > 0, \quad (3.30)$$

along with the I.C.

$$[C(0)] = 0, \quad \begin{cases} \eta(x_T^c, y_T^c, \alpha, \beta, t = 0) = +1 & \text{when } \alpha + \beta < 0 \\ \eta(x_T^c, y_T^c, \alpha, \beta, t = 0) = -1 & \text{when } \alpha + \beta > 0 \end{cases} \quad \forall T \in \tau_h, \quad (3.31)$$

where

$$\begin{aligned} [C(t)] &= [c_1(t), c_2(t), \dots, c_{I+1}(t)]^T, \\ [C_{past}(t)] &= [c_{past,1}(t), c_{past,2}(t), \dots, c_{past,I+1}(t)]^T \end{aligned} \quad (3.32)$$

and

$$[M(t)] = [M_{l,m}]_{1 \leq l, m \leq I+1}, \quad [K] = [K_{l,m}]_{1 \leq l, m \leq I+1} \quad (3.33)$$

with

$$K_{l,m} = \frac{1}{\sigma} \int_S \text{grad} \psi_l \cdot \text{grad} \psi_m \, dx dy, \quad (3.34)$$

$$M_{l,m} = \int_S \hat{\mu}_d(x, y, t, H_h(x, y; t), H_{h,past}(x, y; t)) \psi_l \psi_m \, dx dy, \quad (3.35)$$

and moreover

$$[F(t)] = \frac{d\phi}{dt} [0, 0, \dots, 0, 1]^T. \quad (3.36)$$

In the last equation we used (3.25) and the fact that $\psi_1, \psi_2, \dots, \psi_I$ all vanish on ∂S .

Case of RPM

Proceeding in a similar way, the IVP for $H_h(x, y, t) \simeq H(x, y, t)$ shows the same form as (3.30)-(3.31), however with the mass, stiffness and force matrix now being defined by

$$[M(t)] = [M_{lm}]_{1 \leq l, m \leq I+1}, \quad M_{lm} = \int_S \hat{\mu}_{rev} \psi_l \psi_m dx dy, \quad (3.37)$$

$$[K(t)] = [K_{lm}]_{1 \leq l, m \leq I+1}, \quad K_{lm} = \frac{1}{\sigma} \int_S grad \psi_l grad \psi_m dx dy + \int_S \hat{k}_1(x, y, t) \psi_l \psi_m dx dy, \quad (3.38)$$

$$[F(t)] = [F_l]_{1 \leq l \leq I+1}, \quad F_l = \int_S \hat{k}_2(x, y, t) \psi_l dx dy + \frac{d\phi}{dt} \delta_{l(I+1)}. \quad (3.39)$$

Here, for $g = \mu_{rev}$, $g = k_1$ and $g = k_2$, we put

$$\hat{g}(x, t) = g(x_T^c, y_T^c, t), \quad \forall (x, y) \in T, \quad \forall T \in \tau_h. \quad (3.40)$$

For brevity we denoted

$$\hat{k}_1(x, y, t) = \hat{k}_1(H_h(x, y, t), H_{h,past}(x, y, t)) \quad (3.41)$$

and similarly for $\hat{k}_2(x, t)$.

3.4.2 Field problem in a yoke cross section S

As mentioned above, by introducing the new unknown $\hat{H}(r, z, t) = rH(r, z, t)$, the magnetic field problem in a cross section $S = \{(r, z) | 0 < r_1 < r < r_2, z_1 < z < z_2\}$ of a yoke, has been given a variational formulation similar to the problem (3.18),(3.10) for $H(x, y; t)$ in the cross section of a tooth. Formally, the only modification required is due to the smooth weight factor $\frac{1}{r}$ in the integrand.

In particular, for the IVPs, when allowing for non-linear effects or hysteresis effects, it must be noted that in the CPM case, the evaluation of $\hat{\mu}_d$ rest upon H_h and its history instead of \hat{H}_h and its history. Similarly, in the RPM case, the evaluation of $\hat{\mu}_{rev}$, \hat{k}_1 , \hat{k}_2 rest upon H_h and its history.

3.5 A modified θ -family of finite difference discretisations in time and an iterative procedure

We only discuss the time discretisation of the IVPs (3.30), (3.31), (3.34)-(3.36) and (3.30), (3.31), (3.37)-(3.39), resulting from the FEM for the field problems in a *tooth* cross section. The IVPs resulting from the FEM for the field problem in a *yoke* cross section may be discretised in a similar way. We recall that the underlying variational formulations took a similar form as in the case of a tooth cross section, when passing to a suitably chosen new unknown.

Case of CPM

To take properly into account the jump discontinuities of μ_d with respect to time, we outline a modified θ -family of FDMs in time for the problem (3.30)-(3.31), $0 \leq \theta \leq 1$.

Let Δt be a time step and $t_l = l\Delta t$, ($l = 0, 1, 2, \dots$), be the corresponding equidistant time points.

We define an approximation $H_l^*(x, y)$ of $H_h(x, y, t_l)$, explicitly

$$H_l^*(x, y) \equiv \sum_{i=1}^{I+1} c_i^{(l)} \psi_i(x, y) \simeq \sum_{i=1}^{I+1} c_i(t_l) \psi_i(x, y) \equiv H_h(x, y, t_l), \quad (3.42)$$

by means of a recurrent set of nonlinear systems for $[C^{(l)}] = [c_1^{(l)}, c_2^{(l)}, \dots, c_{I+1}^{(l)}]^T$, similar to (2.51)-(2.52).

Now, the stiffness matrix K take the form (3.34), while the mass matrix is approximated by

$$\tilde{M}_{ij} = \int_S \tilde{\mu}_d(x, y, t, H_h(x, y, t), H_{h,past}(x, y, t)) \psi_i \psi_j dx dy, \quad (3.43)$$

and the appearing column matrix $[H_{ext}^{(l+1)}]$ is defined in a similar way as (2.47)-(2.48), explicitly

$$H_{ext,r}^{(l+1)} = \begin{cases} g_{T,t_l} & : \text{if there is a jump of } \tilde{\mu}_d(x, t) \text{ in one of} \\ & \text{the triangles } \Gamma \text{ sharing the node } r \text{ in} \\ & [t_l, t_{l+1}], \\ \frac{1}{2}[c_r^{(l+1)} + c_r^{(l)}] & : \text{in the other cases.} \end{cases} \quad (3.44)$$

Case of RPM

Let again $0 \leq \theta \leq 1$ be a parameter. We now introduce an approximation $H_l^*(x, y)$ of $H_h(x, y, t_l)$, viz

$$H_l^*(x, y) = \sum_{i=1}^{I+1} c_i^{(l)} \psi_i(x, y), \quad (3.45)$$

by means of the following recurrent set of algebraic systems for $[C^{(l)}] = [c_1^{(l)}, \dots, c_{I+1}^{(l)}]^T$, $l = 0, 1, 2, \dots$,

$$\begin{aligned} \left(\frac{[\tilde{M}^{(l+1)}]}{\Delta t} + \theta[\tilde{K}^{(l+1)}] \right) [C^{(l+1)}] &= \left(\frac{[\tilde{M}^{(l+1)}]}{\Delta t} - (1 - \theta)[\tilde{K}^{(l)}] \right) [C^{(l)}] \\ &+ \theta[\tilde{F}^{(l+1)}] + (1 - \theta)[\tilde{F}^{(l)}], \end{aligned} \quad (3.46)$$

starting from

$$[C^{(0)}] = 0. \quad (3.47)$$

Here, the approximated mass matrix $[\tilde{M}^{(l)}] \simeq [M(t_l)]$, stiffness matrix $[\tilde{K}^{(l)}] \simeq [K(t_l)]$ and force matrix $[\tilde{F}^{(l)}] \simeq [F(t_l)]$ are defined by

$$\tilde{M}_{ij}^{(l)} = \int_S \tilde{\mu}_{rev}^{(l)} \psi_i \psi_j dx dy, \quad (3.48)$$

$$\tilde{K}_{ij}^{(l)} = \frac{1}{\sigma} \int_S \text{grad}\psi_i \cdot \text{grad}\psi_j dx dy + \int_S \tilde{k}_1^{(l)}(x, y) \psi_i \psi_j dx dy, \quad (3.49)$$

$$\tilde{F}_j^{(l)} = \int_S \tilde{k}_2^{(l)}(x, y) \psi_j dx dy + \frac{d\phi}{dt} \delta_{j(I+1)}, \quad (3.50)$$

with

$$\tilde{\mu}_{rev}^{(l)} = (1 - \theta) \hat{\mu}_{rev}(H_{l-1}^*(x, y)) + \theta \hat{\mu}_{rev}(H_l^*(x, y)). \quad (3.51)$$

Moreover $\tilde{k}_1^{(l)}(x, y)$, appearing in (3.49), is the approximation of $\hat{k}_1(x, y, t_l)$, (3.41), which is found when we use $H_p^*(x, y)$, $1 \leq p \leq l$, to describe the dependency on the magnetic field and its history up to $t = t_l$; $\tilde{k}_2^{(l)}(x, y)$ is obtained in a similar way.

As the mass, stiffness and force matrices, entering (3.46), all depend on the unknown, as just mentioned, we again set up a Newton-Raphson iterative procedure to solve the nonlinear system (3.46) at every time point t_l .

3.6 Computational aspects

In practice, the construction of the mass matrices M and the stiffness matrices K , entering the IVPs that results from the FEM, only requires an adaption of a standard technique for BVPs with a *classical* Neumann condition throughout ∂S , see [2] and [3].

This attractive feature follows from the proper choice of the basis function ψ_{I+1} , (3.24). Indeed, return to the basis $(\varphi_j)_{j=1}^J$ of X_h , (3.22), and denote

$$M_{l,m}^{(cl)} = \int_S \hat{g} \varphi_l \varphi_m dx dy, \quad 1 \leq l, m \leq J \quad (3.52)$$

where

$$\hat{g} = \begin{cases} \hat{\mu}_d & \text{in the CPM-case} \\ \hat{\mu}_{rev} & \text{in the RPM-case} \end{cases}, \quad (3.53)$$

Then, we have for the (symmetric) mass matrix M ,

$$M_{l,m} = M_{l,m}^{(cl)} \quad \text{for } 1 \leq l, m \leq I, \quad (3.54)$$

$$M_{l,I+1} = \sum_{k=I+1}^J M_{l,k}^{(cl)} \quad \text{for } 1 \leq l \leq I, \quad (3.55)$$

and

$$M_{I+1,I+1} = \sum_{k=I+1}^J \sum_{r=I+1}^J M_{r,k}^{(cl)}. \quad (3.56)$$

Thus, the assembling of the *global* mass matrix from the *local* element mass matrices, has to be modified as compared to the standard construction of $[M^{(cl)}]$, see e.g. [3], as follows: in the Boolean selection matrices associated to the triangles adjacent to ∂S , the nodes which belong to ∂S must all be treated as one single node. The same remark applies to the stiffness matrix K . Similarly, in the case of RPM, the actual force matrix may be constructed out of the classical force matrix in a simple way.

3.7 Numerical results

The effectiveness and the reliability of the variational approximation method for the problem (3.1)-(3.5), as outlined in the previous sections, has been confirmed by several numerical experiments, both for the yoke and the tooth. Thus, Example 1 illustrates the reliability of the method, by comparison with results from a common 1D model, while Example 2 shows that the approach is effective for the evaluation of the physical quantity, we are looking for. In the numerical examples we have taken a quadratic finite element mesh similar to the one of Fig. 3.4 (with 348 triangular elements), while $\Delta t = \frac{1}{400f}$, (f being introduced below). Again we have taken $\theta = 0.5$ in Section 3.5.

Example 1: Recovery of the electromagnetic loss in a tooth, calculated from the 1D model.

We consider a linear model, with $\mu_d = 2000\mu_0$ [H/m], $\mu_0 = 4\pi 10^{-7}$ and $\sigma = 30^{-1}10^8$ [S/m], for a tooth with cross section as shown in Fig.3.5, for the cases $2d = 0.35$ mm, $2d = 0.50$ mm and $2d = 0.65$ mm.

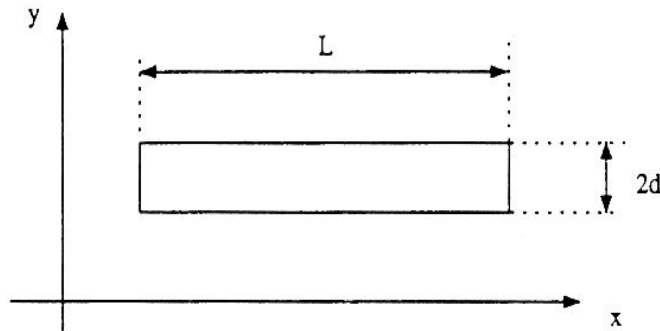


Figure 3.5: The cross section S of the tooth with width $2d$ and length L

The enforced flux is:

$$\phi = 2dLB_{av}\sin(2\pi ft), \quad (3.57)$$

where $B_{av} = 1$ T and $f = 50$ Hz.

In Fig.3.6, the electromagnetic loss E , defined by (3.6), with $T_2 - T_1 = \frac{1}{f}$, is plotted versus $\Delta = \frac{L}{2d}$. For increasing Δ (i.e. for increasing length relative to the width) the computed values of E tend to these obtained by the 1D model, as it should.

Example 2: Evaluation of the electromagnetic loss in a yoke (with increasing curvature)

According to (3.6) the electromagnetic loss over one time period is given by:

$$E = \oint^+ C_b(\phi)d\phi \quad (3.58)$$

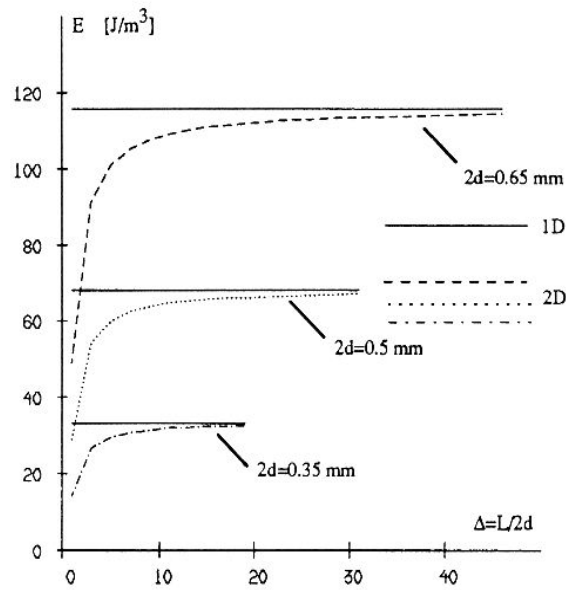


Figure 3.6: *The electromagnetic loss versus $\Delta = \frac{L}{2d}$*

We now consider the axi-symmetric model, with hysteresis effects, of the magnetic field in a cross section of a yoke, shown in Fig.3.7, with $2d = 0.5 \text{ mm}$ and $r_2 - r_1 = 1 \text{ cm}$. We retain $\sigma = 30^{-1}10^8 \text{ [S/m]}$. μ_d is derived from the Preisach model, directly using the experimentally obtained distribution function $P(\alpha, \beta)$, as described in [12] (in contrast to [13], where an approximating analytical expression for $P(\alpha, \beta)$ is constructed, based upon data fitting). Furthermore we retain $f = 50 \text{ Hz}$.

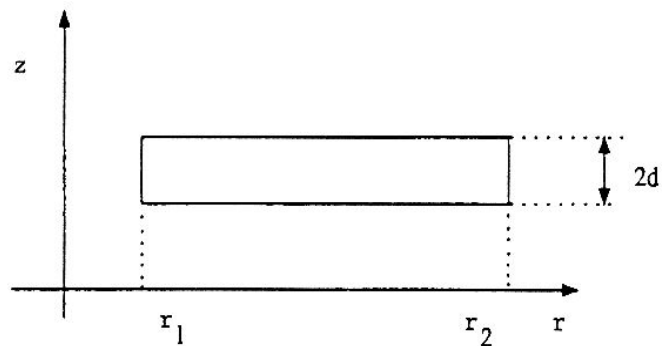
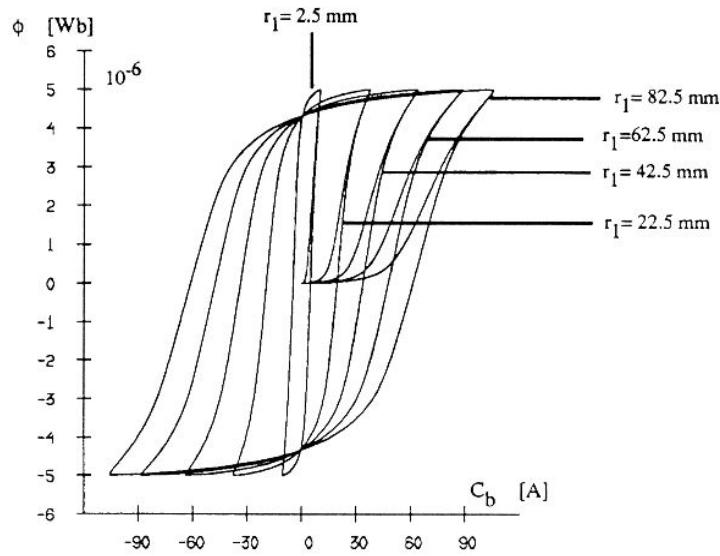


Figure 3.7: *The cross section S of the yoke*

Figure 3.8: (C_b, ϕ) -loops

$r_1(m)$	E (J)	E_v (J)
0.0025	0.00014878	1.5095
0.0225	0.00055418	1.5334
0.0425	0.00096351	1.5435
0.0625	0.00135212	1.5243
0.0825	0.00175755	1.5285

Table 1: *Electromagnetic loss E and energy loss density E_v*

In Fig.3.8, C_b (i.e. the constant value of \hat{H} on ∂S) is plotted versus the enforced flux for different values of r_1 , viz $r_1 = 0.0025$; $r_1 = 0.0225$; $r_1 = 0.0425$; $r_1 = 0.0625$; $r_1 = 0.0825$. The surface enclosed by the respective (C_b, ϕ) -loops is a measure of the electromagnetic loss E , (3.58), shown in Table 1. For physical reasons it can be expected that for increasing r_1 (with retaining $r_2 = r_1 + 1$) the influence of this radius (curvature of the yoke) on the energy loss density becomes neglectible. This is confirmed by our numerical experiment, summarized in the $E_v(J)$ -column of Table 1.

4 A 1D nonlinear Parabolic Problem - use of a vector hysteresis model

4.1 A motivating physical problem and its mathematical model

The magnetic behaviour of ferromagnetic laminations can be described in terms of the macroscopic fields, taking into account the interacting hysteresis and eddy current phenomena.

We consider a single lamination of length l , width w and thickness $2d$, see Fig.4.1. Throughout the sheet, which is assumed isotropic, the time dependent total flux vector $\bar{\phi}(t)$ flows parallel to the (x,y) -plane. Thus the magnetic field and the magnetic induction take the form $\bar{H}=H_x\bar{1}_x+H_y\bar{1}_y$ and $\bar{B}=B_x\bar{1}_x+B_y\bar{1}_y$, respectively. As $d \ll w$ and $d \ll l$, eliminating the edge effects, we may assume H_x , H_y and B_x , B_y to vary in the z -direction only.

Next, we recall the relation $\bar{J} = \sigma \bar{E}$, (1.50), between the electric field \bar{E} and the current density \bar{J} (both parallel to the (x,y) -plane) and we eliminate these vectors from the relevant Maxwell equations (1.43)-(1.45). We arrive at the governing DEs for the magnetic field $\bar{H}(z, t)$, $0 \leq z \leq d$, $t \geq 0$:

$$\frac{1}{\sigma} \frac{\partial^2 H_x}{\partial z^2} = \frac{\partial B_x}{\partial t}, \quad 0 < z < d, \quad t > 0, \quad (4.1)$$

$$\frac{1}{\sigma} \frac{\partial^2 H_y}{\partial z^2} = \frac{\partial B_y}{\partial t}, \quad 0 < z < d, \quad t > 0, \quad (4.2)$$

along with the BCs

$$\frac{\partial H_x}{\partial z}(z = 0, t) = \frac{\partial H_y}{\partial z}(z = 0, t) = 0, \quad t > 0, \quad (4.3)$$

$$\frac{\partial H_x}{\partial z}(z = d, t) = \frac{\sigma}{2} \frac{d\phi_x}{dt}, \quad t > 0, \quad (4.4)$$

$$\frac{\partial H_y}{\partial z}(z = d, t) = \frac{\sigma}{2} \frac{d\phi_y}{dt}, \quad t > 0 \quad (4.5)$$

and the ICs

$$H_x(z, t = 0) = 0, \quad H_y(z, t = 0) = 0, \quad 0 < z < d. \quad (4.6)$$

The BCs (4.3) reflect the symmetry in the lamination. The BCs (4.4) and (4.5) follow when combining (4.1) and (4.2), respectively, with that symmetry and with the definition of the flux, viz

$$\bar{\phi}(t) = \phi_x(t)\bar{1}_x + \phi_y(t)\bar{1}_y, \quad (4.7)$$

where

$$\phi_x(t) = \frac{1}{l} \int_{-d}^d \int_0^l B_x dy dz, \quad \phi_y(t) = \frac{1}{w} \int_{-d}^d \int_0^w B_y dx dz. \quad (4.8)$$

The ICs (4.6) correspond to the demagnetized state of the material.

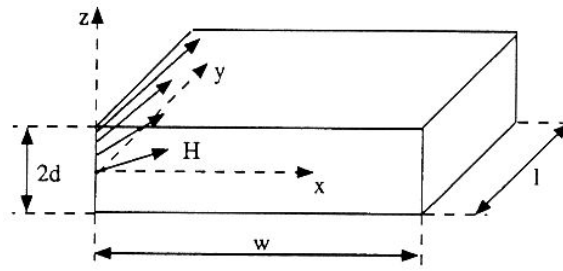
In (4.1)-(4.2), the magnetic induction \bar{B} is related to the magnetic field \bar{H} by the vector Preisach hysteresis model [14].

The total electromagnetic losses per unit volume in the lamination during a time interval $[T_1, T_2]$ are calculated by summing up the hysteresis losses and the eddy current losses, respectively being given by, see e.g. [5],

$$P_h = \frac{1}{2d} \int_{-d}^d dz \int_{T_1}^{T_2} (H_x \frac{\partial B_x}{\partial t} + H_y \frac{\partial B_y}{\partial t}) dt, \quad (4.9)$$

and

$$P_e = \frac{1}{2d\sigma} \int_{-d}^d dz \int_{T_1}^{T_2} \left(\left(\frac{\partial H_x}{\partial z} \right)^2 + \left(\frac{\partial H_y}{\partial z} \right)^2 \right) dt. \quad (4.10)$$


 Figure 4.1: *Magneto-dynamic model of one lamination*

4.2 The vector Preisach theory

4.2.1 Scalar Preisach Model

The BH -relation can be described by a scalar Preisach model if \bar{H} and \bar{B} are unidirectional.

We recall that in the classical rate-independent Preisach model, as briefly discussed in Section 2.2, the material is assumed to consist of small dipoles, each being characterized by a rectangular hysteresis loop as shown in Fig.2.2 (dotted line), [6]. The magnetisation of the dipole M_d takes the value -1 or $+1$. The characteristic parameters α and β are distributed statistically according to a Preisach function $P_s(\alpha, \beta)$.

Denoting the magnitude of the induction vector \bar{B} and of the magnetic field vector \bar{H} by $B=|\bar{B}|$ and by $H=|\bar{H}|$ respectively, the BH -relation is given by, cf. (2.13),

$$B(H, H_{past}) = \frac{1}{2} \int_{-H_m}^{H_m} d\alpha \int_{-H_m}^{\alpha} d\beta \eta_s(\alpha, \beta, t) P_s(\alpha, \beta), \quad (4.11)$$

Here, $\eta_s(\alpha, \beta, t)$ takes the time dependent value of the magnetisation M_d of the dipole with parameters α and β . Consequently, the induction B depends upon the magnetic field $H(t)$ and its history, denoted by $H_{past}(t)$.

4.2.2 Vector Preisach model

In the magnetodynamic model of one lamination, the magnetic field \bar{H} may rotate in a plane parallel to the (x, y) -plane. Therefore, we must pass to a vector hysteresis model.

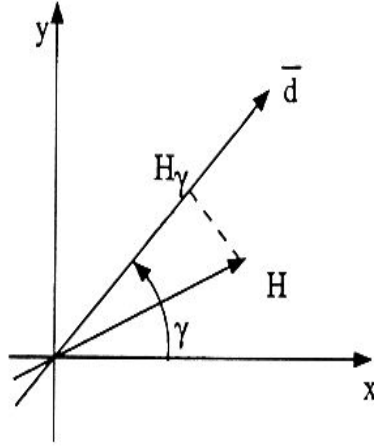
In such a model, as described in [14], the vector \bar{H} is projected on an axis \bar{d} , which encloses an angle γ with the fixed x -axis, $-\frac{\pi}{2} < \gamma < \frac{\pi}{2}$, see Fig.4.2. The corresponding value

$$H_\gamma = H_x \cos \gamma + H_y \sin \gamma \quad (4.12)$$

is taken to be the input of a scalar Preisach model on the axis \bar{d} .

The BH -relation is now given by [15]

$$\bar{B}(\bar{H}, \bar{H}_{past}) = \frac{1}{\pi} \int_{-\frac{\pi}{2}}^{\frac{\pi}{2}} d\gamma B_\gamma(H_\gamma, H_{past, \gamma}) \bar{1}_\gamma, \quad (4.13)$$

Figure 4.2: *Vector Preisach model*

with

$$B_\gamma(H_\gamma, H_{past,\gamma}) = \int_{-H_m}^{H_m} d\alpha \int_{-H_m}^{\alpha} d\beta \eta_r(\gamma, \alpha, \beta, t) P_r(\alpha, \beta), \quad (4.14)$$

where $\eta_r(\gamma, \alpha, \beta, t)$ is obtained from the component H_γ , and thus depends on $\bar{H}(t)$ and $\bar{H}_{past}(t)$. The Preisach function P_r used in this rotational model can be obtained from the function P_s , entering (4.11). From (4.12)-(4.14) we infer that the differential permeabilities $\mu_{xx} = \partial B_x / \partial H_x$, $\mu_{xy} = \partial B_x / \partial H_y$, ..., are given by

$$\begin{aligned} \mu_{xx} &= \frac{1}{\pi} \int_{-\pi/2}^{\pi/2} \mu_\gamma(H_\gamma, H_{past,\gamma}) \cos^2 \gamma d\gamma, \\ \mu_{xy} &= \frac{1}{\pi} \int_{-\pi/2}^{\pi/2} \mu_\gamma(H_\gamma, H_{past,\gamma}) \cos \gamma \sin \gamma d\gamma, \text{ etc.} \end{aligned} \quad (4.15)$$

where, similar to (2.16),

$$\mu_\gamma = \frac{\partial B_\gamma}{\partial H_\gamma} \quad (4.16)$$

is the differential permeability in the scalar Preisach model that corresponds to the axis \bar{d} .

4.2.3 Relation between $\frac{dB}{dt}$ and H

In view of the magnetodynamic model (4.1)-(4.2), $\frac{\partial B_x}{\partial t}$ and $\frac{\partial B_y}{\partial t}$ must be related to the magnetic field $\bar{H}(t)$. For the vector Preisach model one simply has

$$\frac{\partial B_x}{\partial t} = \mu_{xx}(\bar{H}, \bar{H}_{past}) \frac{\partial H_x}{\partial t} + \mu_{xy}(\bar{H}, \bar{H}_{past}) \frac{\partial H_y}{\partial t}, \quad (4.17)$$

$$\frac{\partial B_y}{\partial t} = \mu_{yx}(\bar{H}, \bar{H}_{past}) \frac{\partial H_x}{\partial t} + \mu_{yy}(\bar{H}, \bar{H}_{past}) \frac{\partial H_y}{\partial t}. \quad (4.18)$$

4.3 Combined magnetodynamic model - hysteresis model

Combining (4.17) and (4.18) with (4.1) and (4.2) respectively, we get

$$\frac{1}{\sigma} \frac{\partial^2 H_x}{\partial z^2} = \mu_{xx}(\bar{H}, \bar{H}_{past}) \frac{\partial H_x}{\partial t} + \mu_{xy}(\bar{H}, \bar{H}_{past}) \frac{\partial H_y}{\partial t}, \quad 0 < z < d, \quad t > 0, \quad (4.19)$$

$$\frac{1}{\sigma} \frac{\partial^2 H_y}{\partial z^2} = \mu_{yx}(\bar{H}, \bar{H}_{past}) \frac{\partial H_x}{\partial t} + \mu_{yy}(\bar{H}, \bar{H}_{past}) \frac{\partial H_y}{\partial t}, \quad 0 < z < d, \quad t > 0, \quad (4.20)$$

where now μ_{xx} , μ_{xy} , μ_{yx} and μ_{yy} also depend on the space variable, through $\bar{H}(z, t)$ and $\bar{H}_{past}(z, t)$.

As stated above, to these respective governing DEs for $\bar{H}(z, t)$, we add the BCs (4.3)-(4.5). Finally, the IC will be taken to be

$$H_x(z, t = 0) = 0, \quad H_y(z, t = 0) = 0,$$

$$\begin{cases} \eta_r(\gamma, z, \alpha, \beta, t = 0) = +1 & : \alpha + \beta < 0 \\ \eta_r(\gamma, z, \alpha, \beta, t = 0) = -1 & : \alpha + \beta > 0 \end{cases}, \quad -d < z < d, \quad -\frac{\pi}{2} < \gamma < \frac{\pi}{2}, \quad (4.21)$$

reflecting the chosen initial (demagnetized) state of the material at $t = 0$. Due to the complexity of the material model used, (4.19)-(4.20) constitutes a system of highly nonlinear coupled PDEs with memory.

4.4 Variational formulation

Proceeding similarly as before, the BVP above leads to the following variational problem:

Find the functions $H_x(z, t)$, $H_y(z, t)$, which for each $t > 0$ fulfill that $H_x(\cdot, t)$ and $H_y(\cdot, t) \in W_2^1(]0, d[)$, with $\frac{\partial H_x(\cdot, t)}{\partial t}$ and $\frac{\partial H_y(\cdot, t)}{\partial t} \in L_2(]0, d[)$, and which moreover obey

$$\begin{aligned} & \frac{1}{\sigma} \int_0^d \frac{\partial H_x(z, t)}{\partial z} \frac{dw(z)}{dz} dz + \int_0^d \mu_{xx} \frac{\partial H_x(z, t)}{\partial t} w(z) dz \\ & + \int_0^d \mu_{xy} \frac{\partial H_y(z, t)}{\partial t} w(z) dz = \frac{w(d)}{2} \frac{d\phi_x}{dt}, \quad \forall w \in W_2^1(]0, d[), \quad \forall t > 0 \end{aligned} \quad (4.22)$$

and

$$\begin{aligned} & \frac{1}{\sigma} \int_0^d \frac{\partial H_y(z, t)}{\partial z} \frac{dw(z)}{dz} dz + \int_0^d \mu_{yx} \frac{\partial H_x(z, t)}{\partial t} w(z) dz \\ & + \int_0^d \mu_{yy} \frac{\partial H_y(z, t)}{\partial t} w(z) dz = \frac{w(d)}{2} \frac{d\phi_y}{dt}, \quad \forall w \in W_2^1(]0, d[), \quad \forall t > 0 \end{aligned} \quad (4.23)$$

along with the IC (4.21).

This variational problem may be shown to be formally equivalent with the original BVP (4.19)-(4.20), (4.3)-(4.5) and (4.21).

4.5 Fully discrete numerical scheme

The variational problem (4.22)-(4.23) is solved numerically. We combine (a) a finite element method using quadratic interpolation functions for the discretisation in space, (b) a suitable Crank-Nicholson finite difference scheme for the time discretisation, (c) a numerical quadrature formula with equidistant nodes for the integration over the angle γ in (4.13).

A major computational difficulty in the *discretisation* arises from the hysteresis behaviour of the material, reflected in the dependency of the functions $\mu_{xx}, \dots, \mu_{yy}$ on the vector $\bar{H}_{past}(t)$ (as well as on $\bar{H}(t)$ itself).

4.5.1 Space discretisation by a FEM

We retain the partition $0 \equiv z_1 < z_2 < \dots < z_{2n} < z_{2n+1} \equiv d$ of $[0, d]$ with $2n+1$ equidistant nodes, as in Section 2.5. We also consider the same approximation space W_h , (2.26), and its canonical basis (2.27).

We consider the FE-approximation of (4.22)-(4.23) by determining the functions $H_{x,h}(z, t)$ and $H_{y,h}(z, t)$ of the form,

$$H_{x,h}(z, t) = \sum_{i=1}^{2n+1} c_{x,i}(t) \varphi_i(z), \quad z \in [0, d], \quad t \geq 0, \quad (4.24)$$

$$H_{y,h}(z, t) = \sum_{i=1}^{2n+1} c_{y,i}(t) \varphi_i(z), \quad z \in [0, d], \quad t \geq 0, \quad (4.25)$$

which obeys the discrete version of (4.22)-(4.23), viz

$$\begin{aligned} & \frac{1}{\sigma} \int_0^d \frac{\partial H_{x,h}(z, t)}{\partial z} \frac{dw(z)}{dz} dz + \int_0^d \hat{\mu}_{xx} \frac{\partial H_{x,h}(z, t)}{\partial t} w(z) dz \\ & + \int_0^d \hat{\mu}_{xy} \frac{\partial H_{y,h}(z, t)}{\partial t} w(z) dz = \frac{w(d)}{2} \frac{d\phi_x}{dt}, \quad \forall w \in W_h, \forall t > 0, \end{aligned} \quad (4.26)$$

and

$$\begin{aligned} & \frac{1}{\sigma} \int_0^d \frac{\partial H_{y,h}(z, t)}{\partial z} \cdot \frac{dw(z)}{dz} dz + \int_0^d \hat{\mu}_{yx} \frac{\partial H_{x,h}(z, t)}{\partial t} w(z) dz \\ & + \int_0^d \hat{\mu}_{yy} \frac{\partial H_{y,h}(z, t)}{\partial t} w(z) dz = \frac{w(d)}{2} \frac{d\phi_y}{dt}, \quad \forall w \in W_h, \forall t > 0. \end{aligned} \quad (4.27)$$

along with

$$H_{x,h}(z, t = 0) = 0, \quad H_{y,h}(z, t = 0) = 0,$$

$$\begin{cases} \eta_r(\gamma, z_{2s}, \alpha, \beta, t = 0) = +1 & : \alpha + \beta < 0 \\ \eta_r(\gamma, z_{2s}, \alpha, \beta, t = 0) = -1 & : \alpha + \beta > 0 \end{cases}, \quad 1 \leq s \leq n, \quad -\frac{\pi}{2} < \gamma < \frac{\pi}{2}. \quad (4.28)$$

Here, we have approximated the space dependency of the differential permeability μ_g by passing to $\hat{\mu}_g$, introduced by

$$\hat{\mu}_g(z, t) = \mu_g(z_{2s}, \bar{H}_h(z_{2s}, t), \bar{H}_{h,past}(z_{2s}, t)),$$

$$z_{2s-1} \leq z \leq z_{2s+1}, 1 \leq s \leq n, t > 0, \quad (4.29)$$

with the index g referring to xx , xy , etc, and with \bar{H}_h and $\bar{H}_{past,h}$ being defined by

$$\bar{H}_h = H_{x,h} \bar{1}_x + H_{y,h} \bar{1}_y; \text{ etc.} \quad (4.30)$$

The resulting IVP for the nodal values $H_{x,h}(z_i, t) \equiv c_{x,i}(t)$ and $H_{y,h}(z_i, t) \equiv c_{y,i}(t)$ $t > 0$, reads:

Find the column matrices $[C_x(t)] = [c_{x,1}(t), \dots, c_{x,2n+1}(t)]^T$ and $[C_y(t)] = [c_{y,1}(t), \dots, c_{y,2n+1}(t)]^T$ which obey

$$\begin{bmatrix} M_{xx} & M_{xy} \\ M_{yx} & M_{yy} \end{bmatrix} \frac{d}{dt} \begin{bmatrix} H_{x,h} \\ H_{y,h} \end{bmatrix} + \begin{bmatrix} K & 0 \\ 0 & K \end{bmatrix} \begin{bmatrix} H_{x,h} \\ H_{y,h} \end{bmatrix} = \begin{bmatrix} F_x \\ F_y \end{bmatrix}, \quad (4.31)$$

along with

$$[C_x(0)] = 0, [C_y(0)] = 0, \begin{cases} \eta_r(\gamma, z_{2s}, \alpha, \beta, t = 0) = +1 & \text{when } \alpha + \beta < 0 \\ \eta_r(\gamma, z_{2s}, \alpha, \beta, t = 0) = -1 & \text{when } \alpha + \beta > 0 \end{cases}, \\ -\frac{\pi}{2} < \gamma < \frac{\pi}{2}, 1 \leq s \leq n. \quad (4.32)$$

Here, the block mass matrix entering (4.31) is defined by

$$(M_{xx})_{ij} = \int_0^d \hat{\mu}_{xx} \varphi_i \varphi_j dz, \quad i \text{ and } j = 1, 2, \dots, 2n+1; \quad \text{etc.} \quad (4.33)$$

The block $[K] = [K_{ij}]_{1 \leq i, j \leq 2n+1}$ in the total stiffness matrix that enters (4.31), is defined by

$$(K)_{ij} = \int_0^d \frac{1}{\sigma} \frac{d\varphi_i}{dz} \frac{d\varphi_j}{dz} dz. \quad (4.34)$$

Moreover the total force matrix $[F_x(t) \ F_y(t)]^T$ is given by

$$[F_x] = \left[0 \ 0 \ \dots \ \frac{1}{2} \frac{d\phi_x}{dt} \right]^T, \quad [F_y] = \left[0 \ 0 \ \dots \ \frac{1}{2} \frac{d\phi_y}{dt} \right]^T. \quad (4.35)$$

4.5.2 Time discretisation by a Crank-Nicholson method

The nonlinear IVP (4.31)-(4.32) will again be solved numerically by a θ -family of finite difference schemes, introduced in Section 1.2, combined with an iterative procedure. The procedure is a bit simpler than the one followed in Section 2.6. Indeed, at a fixed time point t there are only a finite number of possible discontinuity points in the integration interval $[-\frac{\pi}{2}, \frac{\pi}{2}]$ in the expression of (4.15) of $\mu_{xx}, \dots, \mu_{yy}$, not affecting their continuity as a function of time. Let Δt be a time step and let $t_l = l \cdot \Delta t$, $l = 1, 2, 3, 4, \dots$, be the corresponding equidistant time points. We want to define an approximation $H_{xl}^*(z)$ of $H_{x,h}(z, t_l)$ and $H_{yl}^*(z)$ of $H_{y,h}(z, t_l)$, i.e.

$$H_{xl}^*(z) = \sum_{i=1}^{2n+1} c_{x,i}^{(l)} \varphi_i(z) \simeq \sum_{i=1}^{2n+1} c_{x,i}(t_l) \varphi_i(z), \quad (4.36)$$

$$H_{yl}^*(z) = \sum_{i=1}^{2n+1} c_{y,i}^{(l)} \varphi_i(z) \simeq \sum_{i=1}^{2n+1} c_{y,i}(t_l) \varphi_i(z), \quad (4.37)$$

by means of a recurrent set of nonlinear systems for

$$[C_x^{(l)}] = [c_{x,1}^{(l)}, c_{x,2}^{(l)}, \dots, c_{x,2n+1}^{(l)}]^T, \quad l = 1, 2, \dots, \quad (4.38)$$

and

$$[C_y^{(l)}] = [c_{y,1}^{(l)}, c_{y,2}^{(l)}, \dots, c_{y,2n+1}^{(l)}]^T, \quad l = 1, 2, \dots, \quad (4.39)$$

involving a parameter $\theta \in [0, 1]$ of the method.

From (4.31) we get

$$\begin{aligned} \int_{t_l}^{t_{l+1}} \begin{bmatrix} M_{xx} & M_{xy} \\ M_{yx} & M_{yy} \end{bmatrix} \frac{d}{dt} \begin{bmatrix} C_x \\ C_y \end{bmatrix} dt + \int_{t_l}^{t_{l+1}} \begin{bmatrix} K & 0 \\ 0 & K \end{bmatrix} \begin{bmatrix} C_x \\ C_y \end{bmatrix} dt \\ = \int_{t_l}^{t_{l+1}} \begin{bmatrix} F_x \\ F_y \end{bmatrix} dt \end{aligned} \quad (4.40)$$

We approximate the first term as

$$\begin{aligned} \int_{t_l}^{t_{l+1}} \begin{bmatrix} M_{xx} & M_{xy} \\ M_{yx} & M_{yy} \end{bmatrix} \frac{d}{dt} \begin{bmatrix} C_x \\ C_y \end{bmatrix} dt \\ \simeq \begin{bmatrix} \tilde{M}_{xx}^{(l+1)} & \tilde{M}_{xy}^{(l+1)} \\ \tilde{M}_{yx}^{(l+1)} & \tilde{M}_{yy}^{(l+1)} \end{bmatrix} \left(\begin{bmatrix} C_x^{(l+1)} \\ C_y^{(l+1)} \end{bmatrix} - \begin{bmatrix} C_x^{(l)} \\ C_y^{(l)} \end{bmatrix} \right) \end{aligned} \quad (4.41)$$

Here, $\tilde{M}_{xx}^{(l)}$, $\tilde{M}_{xy}^{(l)}$, ..., are defined by

$$\left(\tilde{M}_{xx}^{(l)} \right)_{ij} = \int_0^d \tilde{\mu}_{xx}^{(l)} \varphi_i \varphi_j dz, \quad \text{etc.}, \quad (4.42)$$

with

$$\tilde{\mu}_{xx}^{(l)} = \theta \hat{\mu}_{xx}^{(l)} + (1 - \theta) \hat{\mu}_{xx}^{(l-1)}, \quad (4.43)$$

where $\hat{\mu}_{xx}^{(l)}$ is the approximation of $\hat{\mu}_{xx}(z, t_l)$, (4.29), when we use H_{xp}^* , (4.36), and H_{yp}^* , (4.37), $1 \leq p \leq l$, to describe the dependency on the magnetic field and its history up to $t = t_l$.

We approximate the 2nd and 3rd term of (4.40) as follows

$$\begin{aligned} \int_{t_l}^{t_{l+1}} \begin{bmatrix} K & 0 \\ 0 & K \end{bmatrix} \begin{bmatrix} C_x \\ C_y \end{bmatrix} dt \\ \simeq \begin{bmatrix} K & 0 \\ 0 & K \end{bmatrix} \left(\theta \begin{bmatrix} C_x^{(l+1)} \\ C_y^{(l+1)} \end{bmatrix} + (1 - \theta) \begin{bmatrix} C_x^{(l)} \\ C_y^{(l)} \end{bmatrix} \right) \Delta t \end{aligned} \quad (4.44)$$

and

$$\int_{t_l}^{t_{l+1}} \begin{bmatrix} F_x \\ F_y \end{bmatrix} dt \simeq \left(\theta \begin{bmatrix} F_x(t_{l+1}) \\ F_y(t_{l+1}) \end{bmatrix} + (1 - \theta) \begin{bmatrix} F_x(t_l) \\ F_y(t_l) \end{bmatrix} \right) \Delta t. \quad (4.45)$$

Finally, combining (4.41), (4.44) and (4.45), we get from (4.40)

$$\begin{aligned} \left(\frac{1}{\Delta t} \begin{bmatrix} \tilde{M}_{xx}^{(l+1)} & \tilde{M}_{xy}^{(l+1)} \\ \tilde{M}_{yx}^{(l+1)} & \tilde{M}_{yy}^{(l+1)} \end{bmatrix} + \theta \begin{bmatrix} K & 0 \\ 0 & K \end{bmatrix} \right) \begin{bmatrix} C_x^{(l+1)} \\ C_y^{(l+1)} \end{bmatrix} \\ = \left(\frac{1}{\Delta t} \begin{bmatrix} \tilde{M}_{xx}^{(l+1)} & \tilde{M}_{xy}^{(l+1)} \\ \tilde{M}_{yx}^{(l+1)} & \tilde{M}_{yy}^{(l+1)} \end{bmatrix} - (1 - \theta) \begin{bmatrix} K & 0 \\ 0 & K \end{bmatrix} \right) \begin{bmatrix} C_x^{(l)} \\ C_y^{(l)} \end{bmatrix} \\ + \theta \begin{bmatrix} F_x(t_{l+1}) \\ F_y(t_{l+1}) \end{bmatrix} + (1 - \theta) \begin{bmatrix} F_x(t_l) \\ F_y(t_l) \end{bmatrix}, \quad l = 0, 1, 2, \dots \end{aligned} \quad (4.46)$$

along with, see (4.32),

$$[H_{x,h}^{(0)}] = [H_{y,h}^{(0)}] = 0. \quad (4.47)$$

As the matrices $[\tilde{M}_{xx}^{(l+1)}]$, $[\tilde{M}_{xy}^{(l+1)}]$, etc., depend on the unknown $H_{xp}^*(z)$ and $H_{yp}^*(z)$, $1 \leq p \leq l+1$, (4.36)-(4.37), we set up a Newton-Raphson iteration procedure to solve the nonlinear system (4.46) at each time point $t = t_l$.

4.5.3 Discretisation of the Preisach model

We choose a natural number N and we consider the partition of $[-\pi/2, \pi/2]$ given by $\gamma_s = -\pi/2 + (s-1)\pi/N$, $1 \leq s \leq N$. We then discretize the equation (4.13) by

$$\bar{B}(\bar{H}, \bar{H}_{past}) \simeq \frac{1}{N} \sum_{s=1}^N B_{\gamma_s}(H_{\gamma_s}, H_{past,\gamma_s}) \bar{1}_{\gamma_s} \quad (4.48)$$

where H_{γ_s} and H_{past,γ_s} are the projections of \bar{H} and \bar{H}_{past} , respectively, on the axis \bar{d}_s enclosing an angle γ_s with the x -axis.

Similarly as in (4.15) we now get

$$\mu_{xx} \simeq \frac{1}{N} \sum_{s=1}^N \mu_s \cos^2 \gamma_s, \text{ etc.} \quad (4.49)$$

In practice, a choice of N exceeding 20 is found to give no relevant increase of accuracy.

4.6 Numerical results

We present some numerical results obtained from the combined magnetodynamic model described in Section 4.3. Again in the finite element discretisation we have taken $n=10$ (quadratic) elements, while in the time discretisation, $\Delta t = \frac{T}{400}$, (T being defined below). Again we have taken $\theta = 0.5$ in Section 4.5.2. The magnetic field strength at the outer boundary of the lamination is enforced:

$$\begin{cases} H_x(z = d, t) = H_{x,b} = H_{xmax} \cos\left(\frac{2\pi t}{T}\right) \\ H_y(z = d, t) = H_{y,b} = H_{ymax} \sin\left(\frac{2\pi t}{T}\right) \end{cases} \quad (4.50)$$

Fig.4.3 depicts the average induction $B_{x,a}$ (with respect to z) as a function of the magnetic field strength $H_{x,b}$ at the outer boundary of the lamination under alternating conditions (dashed line) and rotational excitation (full line). In both cases $T=20ms$.

A full validation, similarly as the one in Section 2.7, of the numerical model developed above is not yet possible as experimental results are still lacking. However, several properties, both qualitative and quantitative, of the combined magnetodynamic model - hysteresis model, described above, indicate its reliability and efficiency.

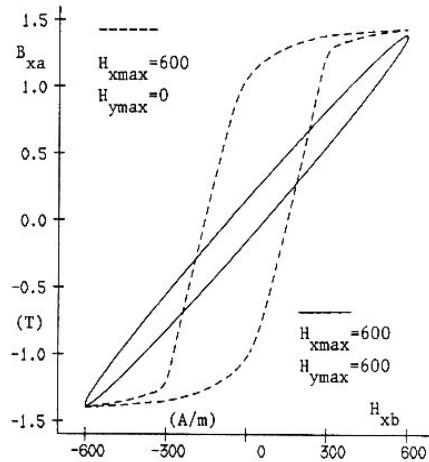


Figure 4.3: *Dynamic $B_{x,a}H_{x,b}$ - and $B_{y,a}H_{y,b}$ -loops under alternating and rotating conditions using the vector hysteresis model*

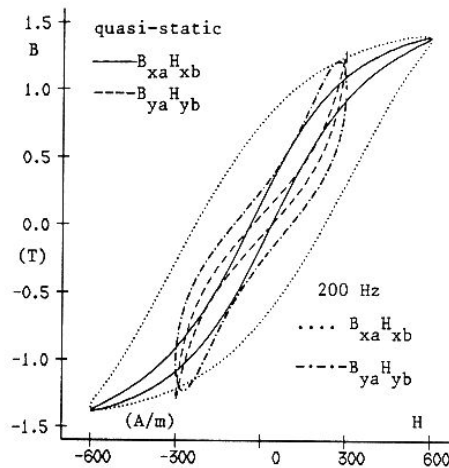


Figure 4.4: *Quasi-static and dynamic $B_{x,a}H_{x,b}$ -, $B_{y,a}H_{y,b}$ -loops under elliptical excitation*

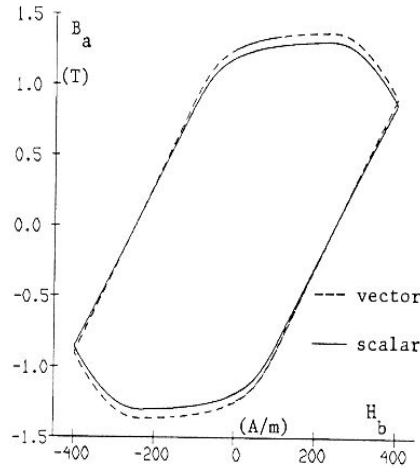


Figure 4.5: *Dynamic $B_{x,a}H_{x,b}$ - and $B_{y,a}H_{y,b}$ -loops under alternating conditions using the model of section 2 and the model of section 4*

For instance, for the limit case of alternating excitation, there is a good agreement with the results obtained from the model of Section 2.3, where a scalar Preisach theory was used. This is shown in Fig.4.5.

At the other hand, Fig.4.4 confirms the enclosed area of the BH-loops to increase with increasing frequency. This reflects the physically evident increase of the electromagnetic losses due to the eddy current effects.

5 A 2D Elliptic Problem - use of a vector hysteresis model

5.1 A motivating physical problem and its mathematical model

We consider a single tooth region, see Fig.5.1, where the electrical conductivity σ now is assumed to be zero. The relevant Maxwell equations for the magnetic field $\vec{H} = H_x \bar{i}_x + H_y \bar{i}_y$ and the magnetic induction $\vec{B} = B_x \bar{i}_x + B_y \bar{i}_y$, in the 2D domain D now read, see (1.43), (1.45),

$$\text{rot} \vec{H} = 0, \quad (5.1)$$

$$\text{div} \vec{B} = 0, \quad (5.2)$$

where the relation between \vec{H} and \vec{B} is again defined by the material characteristics obtained by the vector Preisach hysteresis model, described in Section 4.2.

The boundary ∂D is divided into six parts $\partial D_1, \partial D_2, \dots, \partial D_6$, see again Fig.5.1. We consider a total flux $\phi_s(t)$ through the parts ∂D_s , $s=1,2,3$, which are assumed to be *perfect magnetically conducting* (i.e. $\int_{a_1}^{a_2} \vec{H} \cdot \vec{dl} = 0$ for each couple of points a_1 and a_2 on ∂D_s). Thus we are led to the following BCs

$$\phi_s(t) = \int_{\partial D_s} \vec{B} \cdot \vec{n} dl, \quad t > 0, \quad s = 1, 2, 3, \quad (5.3)$$

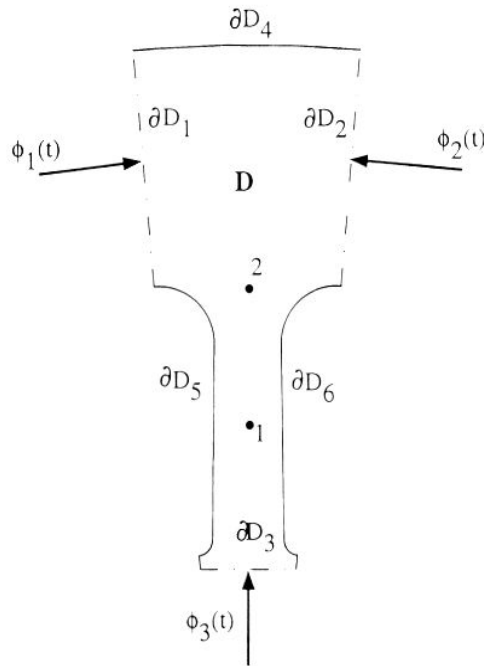


Figure 5.1: Model of one tooth region

and

$$\bar{H}x\bar{n} = \bar{0} \text{ on } \partial D_s, \quad t > 0, \quad s = 1, 2, 3, \quad (5.4)$$

where \bar{n} is the unit outward normal vector to the boundary part ∂D_s .

At the other hand a *zero flux leakage* through ∂D_4 , ∂D_5 and ∂D_6 results in the additional BCs:

$$\bar{B} \cdot \bar{n} = 0 \text{ on } \partial D_s, \quad t > 0, \quad s = 4, 5, 6. \quad (5.5)$$

The demagnetized state of the material at $t = 0$ is expressed by the IC, cf.(4.21),

$$\bar{H}(x, y, t = 0) = 0, \quad \begin{cases} \eta_r(\gamma, x, y, \alpha, \beta, t = 0) = +1 & \text{when } \alpha + \beta < 0 \\ \eta_r(\gamma, x, y, \alpha, \beta, t = 0) = -1 & \text{when } \alpha + \beta > 0 \end{cases}, \\ -\frac{\pi}{2} < \gamma < \frac{\pi}{2}, \quad \forall (x, y) \in D. \quad (5.6)$$

5.2 A nonstandard variational formulation

First, we rewrite the Maxwell equations (5.1)-(5.2) in a suitable form. From (5.1) a scalar potential $\zeta(x, y, t)$ may be introduced such that $\bar{H} = -\text{grad}\zeta$ (of course, ζ can only be determined apart from a constant, the choice of which will be specified below). The Maxwell equation $\text{div}\bar{B} = 0$ can not be rewritten in a manageable way in terms of the scalar potential ζ , entering $\bar{H} = -\text{grad}\zeta$, to take properly into account the material characteristics of the vector Preisach model given by (4.13)-(4.14).

To overcome this difficulty, notice that the differential permeabilities $\mu_{xx} = \partial B_x / \partial H_x$, $\mu_{xy} = \partial B_x / \partial H_y$, $\mu_{yx} = \partial B_y / \partial H_x$ and $\mu_{yy} = \partial B_y / \partial H_y$ are *uniquely* defined by the vector Preisach model. Hence, a suitable reformulation of the problem should incorporate the material characteristics by means of these permeabilities. Therefore, we pass to the auxiliary unknown u , defined as

$$u(x, y, t) = \frac{\partial \zeta}{\partial t}. \quad (5.7)$$

First, from the representation of \bar{H} and from the definition of the permeabilities, we have

$$-\frac{\partial B_x}{\partial t} = \mu_{xx} \frac{\partial u}{\partial x} + \mu_{xy} \frac{\partial u}{\partial y}, \quad (5.8)$$

$$-\frac{\partial B_y}{\partial t} = \mu_{yx} \frac{\partial u}{\partial x} + \mu_{yy} \frac{\partial u}{\partial y}. \quad (5.9)$$

Consequently, (5.2) leads to the elliptic DE for the auxiliary function $u(x, y, t)$, (5.7),

$$\frac{\partial}{\partial x} \left(\mu_{xx} \frac{\partial u}{\partial x} + \mu_{xy} \frac{\partial u}{\partial y} \right) + \frac{\partial}{\partial y} \left(\mu_{yx} \frac{\partial u}{\partial x} + \mu_{yy} \frac{\partial u}{\partial y} \right) = 0, \quad \text{in } S, t > 0(\text{param.}). \quad (5.10)$$

in which the time variable $t > 0$ is only a parameter appearing in the coefficient functions $\mu_{xx}, \dots, \mu_{yy}$. The BCs (5.3), (5.4) and (5.5) respectively imply

$$\frac{d\phi_s(t)}{dt} = \int_{\partial D_s} \frac{d\bar{B}}{dt} \cdot \bar{n} \, dl, \quad t > 0, \quad s = 1, 2, 3 \quad (5.11)$$

$$\zeta = C_s(t) \text{ (constant) on } \partial D_s, \quad t > 0, \quad s = 1, 2, 3 \quad (5.12)$$

and

$$\frac{d\bar{B}}{dt} \cdot \bar{n} = 0 \text{ on } \partial D_s, \quad t > 0, \quad s = 4, 5, 6. \quad (5.13)$$

Here, to remove the degree of freedom involved in the scalar potential ζ , we *choose*

$$\zeta = 0 \text{ on } \partial D_3, \quad t > 0. \quad (5.14)$$

We must add the IC resulting from (5.6) and (5.14), viz

$$\zeta(x, y, t = 0) = 0, \quad \begin{cases} \eta_r(\gamma, x, y, \alpha, \beta, t = 0) = +1 & \text{when } \alpha + \beta < 0 \\ \eta_r(\gamma, x, y, \alpha, \beta, t = 0) = -1 & \text{when } \alpha + \beta > 0 \end{cases}, \quad (5.15)$$

$$-\frac{\pi}{2} < \gamma < \frac{\pi}{2}, \quad \forall (x, y) \in D.$$

Source conditions

Two types of source conditions occur.

(a) With *ϕ -type excitation*, the total flux $\phi_s(t)$ through ∂D_s , $s=1,2,3$ is enforced. On account of (5.2), (5.3) and (5.5) we must require that $\sum_{s=1}^3 \phi_s(t) = 0, t > 0$. Then,

the uniform but time depending value of the scalar potential ζ on ∂D_s , denoted by $C_s(t)$, $s = 1$ or 2 , is *not* given a priori, but must be determined as part of the problem.

(b) With so called ζ -excitation, the uniform value $\zeta(t) = C_s(t)$, $t > 0$, at ∂D_s , $s = 1$ and 2 , is enforced, (recall (5.14)). From the BVP (5.10), (5.12)-(5.13), (5.15), we may obtain the magnetic induction \bar{B} . The total flux $\phi_s(t)$, $s = 1, 2$ or 3 , then follows from (5.11) when we take into account that $\phi_s(t = 0) = 0$ due to (5.15).

To derive a suitable variational form of this problem, we introduce the function space

$$V = \{v \in W_2^1(D); v|_{\partial D_s} \text{ is a constant depending on } s, s = 1, 2, 3\}. \quad (5.16)$$

Here, $W_2^1(D)$ is the usual first order Sobolev space on D and the condition " $v|_{\partial D_s}$ is constant" must be understood in the sense of traces, as defined e.g. in [2]. Multiplying both sides of (5.10) with a test function $v(x, y) \in V$, integrating over D , applying Green's formula (1.21) and invoking the BC (5.11), the problem (5.10)-(5.15) is found to be (formally) equivalent with the following variational problem:

Find a function $\zeta(x, y, t)$, with $u(x, y; t) = \frac{\partial \zeta}{\partial t}$, that shows the property $\zeta \in V$ and $\frac{\partial \zeta}{\partial t} \in L_2(D)$ for every $t > 0$, and obeys

$$\int_D \left[\left(\mu_{xx} \frac{\partial u}{\partial x} + \mu_{xy} \frac{\partial u}{\partial y} \right) \frac{\partial v}{\partial x} + \left(\mu_{yx} \frac{\partial u}{\partial x} + \mu_{yy} \frac{\partial u}{\partial y} \right) \frac{\partial v}{\partial y} \right] dx dy = \sum_{s=1}^3 \frac{d\phi_s(t)}{dt} v|_{\partial D_s} \quad (5.17)$$

$$\forall v \in V, t > 0$$

along with the IC (5.15)

Notice that by the requirement $\zeta \in V$, for every $t > 0$, (5.12) is automatically taken into account.

5.3 A combined FE-FD-discretized vector Preisach model

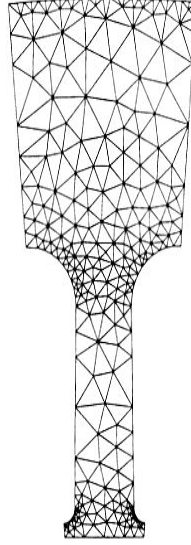
5.3.1 Space discretisation by finite elements

For a usual triangulation τ_h of the domain D , (h mesh parameter), shown in Fig.5.2, we consider a quadratic finite element mesh, as introduced in Section 1.1.

By $\varphi_j(x, y)$, ($j = 1, \dots, J$), we denote the *standard cardinal* basis functions, associated to the nodes (x_j, y_j) , ($j = 1, \dots, J$), J being the total number of nodes. Here, the nodes are numbered such that the first I of them, $I < J$, belong to the domain D or to the boundaries ∂D_4 , ∂D_5 and ∂D_6 . On the boundaries ∂D_1 , ∂D_2 and ∂D_3 we have J_1 , J_2 and J_3 nodes, respectively ($J - I = J_1 + J_2 + J_3$). We introduce the spaces X_h and X_{0h} similarly as in (3.22)-(3.23).

Next we introduce the special functions belonging to X_h :

$$\psi_{I+1}(x, y) = \sum_{j=I+1}^{I+J_1} \varphi_j(x, y), \quad (5.18)$$

Figure 5.2: Triangulation τ_h for the domain D

$$\psi_{I+2}(x, y) = \sum_{j=I+J_1+1}^{I+J_1+J_2} \varphi_j(x, y), \quad (5.19)$$

$$\psi_{I+3}(x, y) = \sum_{j=I+J_1+J_2+1}^J \varphi_j(x, y), \quad (5.20)$$

showing the property

$$\psi_{I+s} \equiv 1 \text{ on } \partial D_s, s = 1, 2, 3. \quad (5.21)$$

Moreover, ψ_{I+s} is readily understood to vanish throughout D apart from the triangles $T \in \tau_h$ adjacent to ∂D_s .

Writing, for convenience, $\psi_j = \varphi_j$, $1 \leq j \leq I$, we finally define the space V_h by:

$$V_h = \text{span}(\psi_j)_{j=1}^{I+3} = X_{0h} \bigoplus \text{span}(\psi_{I+s})_{s=1}^3. \quad (5.22)$$

This space V_h is suitable for a conforming FEM as $V_h \subset V$. Indeed, for $v \in V_h$ one evidently has $v \in X_h \subset W_2^1(D)$, while moreover v is constant on ∂D_1 , ∂D_2 and ∂D_3 , due to (5.21).

The finite element approximation $\zeta_h(x, y; t) \in V_h$ of $\zeta(x, y; t)$ is defined by a variational problem similar to (5.17)-(5.15), now with V replaced by V_h . Here, we approximate the space dependency of μ_{kl} , by passing to $\hat{\mu}_{kl} \simeq \mu_{kl}$, defined by

$$\begin{aligned} & \hat{\mu}_{kl}(x, y, t, \zeta_h(x, y; t), \zeta_{h,past}(x, y; t)) \\ &= \mu_{kl}(x_T^c, y_T^c, t, \zeta_h(x_T^c, y_T^c, t), \zeta_{h,past}(x_T^c, y_T^c, t)), \\ & \forall (x, y) \in T, \forall T \in \tau_h, t > 0, \end{aligned} \quad (5.23)$$

where (x_T^c, y_T^c) is the center of gravity of T . This allows us to take properly into account the nonlinear and hysteresis effects, resulting in the complicated form of the differential permeability μ_{kl} . Here, μ_{kl} now depends upon the finite element approximation $H_h(x, y; t) = -\text{grad}\zeta_h$ and $H_{h,past}(x, y; t) = -\text{grad}\zeta_{h,past}$ of the magnetic field $H(x, y; t)$ and its history $H_{past}(x, y; t)$, respectively.

Explicitly, recalling (5.14) and decomposing φ_h as

$$\zeta_h(x, y; t) = \sum_{j=1}^{I+2} c_j(t) \psi_j(x, y), \quad t > 0, \quad (5.24)$$

we have $c_j(t) = \zeta_h(x_j, y_j; t)$, $1 \leq j \leq I$, and moreover $c(t) = \zeta_h(x, y; t)|_{\partial D_s}$, $s = 1, 2$, due to the proper choice of the basis functions of V_h , (5.22).

Notice that in the case of ϕ -excitation (case (a) in Section 5.2), all coefficient functions $c_j(t)$, $1 \leq j \leq I + 2$, are unknown, while in the case of ζ -excitation (case (b) in Section 5.2), the coefficient functions $c_{I+1}(t)$ and $c_{I+2}(t)$ are given.

These unknown coefficient functions will be derived from a system of first order ODEs, resulting from the finite element *discretisation* of (5.17). More precisely, take as test functions in (5.17) either $v = \psi_i$, $1 \leq i \leq I + 2$ (case (a)), or $v = \psi_i$, $1 \leq i \leq I$, (case (b)). Then, we are led to the following system of ODEs

$$[M(t, C(t), C^{(past)}(t))] \frac{d[C]}{dt} = [F], \quad t > 0, \quad (5.25)$$

along with the ICs, cf. (5.15),

$$[C(0)] = 0 \quad (5.26)$$

and

$$\begin{cases} \eta_r(x, y, \alpha, \beta, t = 0) = +1 & \text{when } \alpha + \beta < 0 \\ \eta_r(x, y, \alpha, \beta, t = 0) = -1 & \text{when } \alpha + \beta > 0 \end{cases}, \quad \forall (x, y) \in D. \quad (5.27)$$

The second IC corresponds to the history of the material at $t=0$ (i.e. the demagnetized state of the material).

Here, the matrices involved read as follows.

case (a): ϕ -type excitation

$[C]$ and $[C^{(past)}]$ are the column matrices,

$$\begin{aligned} [C(t)] &= [c_1(t), c_2(t), \dots, c_{I+2}(t)]^T, \\ [C_{past}(t)] &= [c_{1,past}(t), c_{2,past}(t), \dots, c_{I+2,past}(t)]^T, \end{aligned} \quad (5.28)$$

while $[M]$ is the mass matrix given by

$$[M(t, C(t), C_{past}(t))] = [M_{l,m}]_{1 \leq l, m \leq I+2}, \quad (5.29)$$

with

$$M_{l,m} =$$

$$\int_D \left(\hat{\mu}_{xx} \frac{\partial \psi_l}{\partial x} \frac{\partial \psi_m}{\partial x} + \hat{\mu}_{xy} \frac{\partial \psi_l}{\partial x} \frac{\partial \psi_m}{\partial y} + \hat{\mu}_{yx} \frac{\partial \psi_l}{\partial y} \frac{\partial \psi_m}{\partial x} + \hat{\mu}_{yy} \frac{\partial \psi_l}{\partial y} \frac{\partial \psi_m}{\partial y} \right) dx dy \quad (5.30)$$

Finally, the force matrix $[F]$, corresponding to the RHS of (5.17), is a column matrix with $(I + 2)$ elements, viz

$$[F(t)] = \frac{d\phi_1}{dt} [0, 0, \dots, 0, 1, 0]^T + \frac{d\phi_2}{dt} [0, 0, \dots, 0, 0, 1]^T, \quad (5.31)$$

where we used (5.21) and the fact that $\psi_1, \psi_2, \dots, \psi_I$ all vanish on ∂D_1 and ∂D_2 .

case (b): ζ -type excitation

$[C]$, $[C_{past}]$ and $[M]$ take a similar form as in case (a), of course with the proper dimensions: now in the system (5.25) I equations are left.

The force matrix now has the form

$$[F(t)] = [F_1(t), F_2(t), \dots, F_I(t)]^T \quad (5.32)$$

with

$$F_i(t) = -M_{i,I+1} \frac{d}{dt} c_{I+1}(t) - M_{i,I+2} \frac{d}{dt} c_{I+2}(t), \quad 1 \leq i \leq I. \quad (5.33)$$

in which $c_{I+1}(t) \equiv \zeta_{I+1}(t)$ and $c_{I+2}(t) \equiv \zeta_{I+2}(t)$ are given. (5.33) results from transferring to the RHS of (5.25) the terms containing the known functions $\frac{dc_{I+1}}{dt}$ and $\frac{dc_{I+2}}{dt}$.

5.3.2 Time discretisation by finite differences

The IVP (5.25)-(5.27) is solved numerically by a suitable FDM, extending the classical technique introduced in Section 1.2. We may restrict ourselves to the case of ϕ -excitation, (case (a)), the case of ζ -excitation being completely analogous. The analysis proceeds similarly as in [12].

Let Δt be a time step and let $t_k = k \cdot \Delta t$, ($k = 0, 1, 2, \dots$), be the corresponding equidistant time points. Let $\theta \in [0, 1]$ be a parameter of the method. We define an approximation $C^{(k)} = [c_1^{(k)}, c_2^{(k)}, \dots, c_{I+2}^{(k)}]^T$ of $C(t_k) = [c_1(t_k), c_2(t_k), \dots, c_{I+2}(t_k)]^T$, ($k = 1, 2, \dots$), by the following recurrent set of algebraic systems

$$[\tilde{M}^{(k)}] \frac{[C^{(k)}] - [C^{(k-1)}]}{\Delta t} = \theta [F(t_k)] + (1 - \theta) [F(t_{k-1})], \quad k = 1, 2, \dots \quad (5.34)$$

starting from, see (5.26),

$$[C^{(0)}] = 0. \quad (5.35)$$

Here, the matrix $[\tilde{M}^{(k)}]$ is constructed out of the matrix $[M]$, (5.29)-(5.30), by a *time averaging technique* for the differential permeabilities in the time interval $[t_{k-1}, t_k]$. More precisely, $\hat{\mu}_{xx}$ is replaced by

$$\tilde{\mu}_{xx}^{(k)} = \theta \hat{\mu}_{xx}(t_k) + (1 - \theta) \hat{\mu}_{xx}(t_{k-1}) \quad (5.36)$$

and similarly for $\hat{\mu}_{xy}, \dots, \hat{\mu}_{yy}$.

By means of $[C^{(k)}]$ we construct an approximation $\zeta_h^{(k)}(x, y)$ of $\zeta_h(x, y, t_k)$, (5.24), viz

$$\zeta_h^{(k)}(x, y) = \sum_{j=1}^{I+2} c_j^{(k)} \psi_j(x, y). \quad (5.37)$$

As the matrix $\tilde{M}^{(k)}$ depends on the unknown $C^{(k)}$, we set up an iterative Newton-Raphson procedure to solve the *nonlinear* system (5.34) at every time point t_k , similarly as in (2.51). In practice we take $\theta = 0.5$.

5.4 Numerical results

The effectiveness of the variational approximation method for the problem (5.10)-(5.15), as outlined in the previous section, has been confirmed by several numerical experiments, both for the case of ϕ -excitation and for the case of ζ -excitation. Here, we consider a test problem with practical relevance, viz the evaluation of the local field patterns in one tooth region of an asynchronous machine, shown in Fig.5.1. We used the triangulation shown in Fig.5.2. The time step used was again $\Delta t = \frac{1}{400f}$, (f being introduced below).

The numerical results obtained with the present model are compared with these resulting from more common models based upon a single valued material characteristic. More precisely, we will compare the numerical results for the time variation of \bar{H} and \bar{B} in selected points of the tooth region D . As both the scalar potential excitation and the flux excitation are periodic in time, we may use a complex Fourier decomposition for the local vector fields $\bar{H}(x, y; t)$ and $\bar{B}(x, y; t)$, viz

$$\bar{H}(x, y; t) \equiv \sum_{k=-\infty}^{+\infty} H_k(x, y) \cdot e^{j(k\omega t + \alpha_k)}, \quad (5.38)$$

$$\bar{B}(x, y; t) \equiv \sum_{k=-\infty}^{+\infty} B_k(x, y) \cdot e^{j(k\omega t + \beta_k)}. \quad (5.39)$$

Here, ω is 2π times the basic frequency, α_k [resp. β_k] and H_k [resp. B_k] are the phase angle and the amplitude of the k -th harmonic of \bar{H} [resp. \bar{B}].

For the magnetic material we used the Preisach function P_r which obeys

$$\int_{H_1}^{H_2} d\alpha \int_{H_1}^{\alpha} d\beta P_r(\alpha, \beta) = 13.10^{-6} |H_1 - H_2| \\ + 0.56(q(H_1) - q(H_2))(q(-H_2) - q(-H_1)), -H_m \leq H_1 \leq H_2 \leq H_m \quad (5.40)$$

with

$$q(x) = \arctan(x/200). \quad (5.41)$$

This corresponds to a physically relevant function P_r for an industrial available material, intensively analyzed. We present numerical results for the 2 types of excitation mentioned above.

case 1: ζ -excitation

We enforce a simple time variation of the scalar potential at the boundary parts ∂D_1 and ∂D_2 , viz

$$\zeta_{I+1}(t) = \zeta_{max} \cos(2\pi ft + \gamma_1) \quad (5.42)$$

and

$$\zeta_{I+2}(t) = -\zeta_{max} \cos(2\pi ft + \gamma_2) \quad (5.43)$$

with $\zeta_{max} = 120$, $f = 50Hz$, $\gamma_1 = 25^\circ$ and $\gamma_2 = 6^\circ$.

For this excitation we compute the field pattern in the domain D and we consider point 2 in Fig.5.1. Fig.5.3 reveals the difference between the $B_x B_y$ -loci obtained with the vector Preisach model and the one obtained with the more common single valued material characteristic.

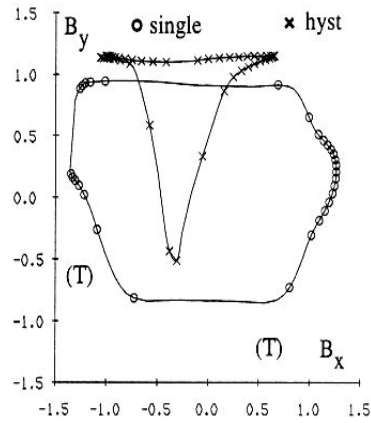


Figure 5.3: $B_x B_y$ -loci in point 2, case 1

Up to now, no measurement set up for rotating magnetic fields are available to the authors to validate experimentally the numerical approach.

case 2: ϕ -excitation

The enforced (realistic) flux patterns through ∂D_1 and ∂D_2 are

$$\phi_j(t) = a_{j,1}\cos(2\pi ft + \gamma_{j,1}) + a_{j,15}\cos(30\pi ft + \gamma_{j,15}) + a_{j,17}\cos(34\pi ft + \gamma_{j,17}),$$

$$j = 1, 2, \quad (5.44)$$

where the amplitudes and phase angles are given in Table 2 and where $f = 50Hz$.

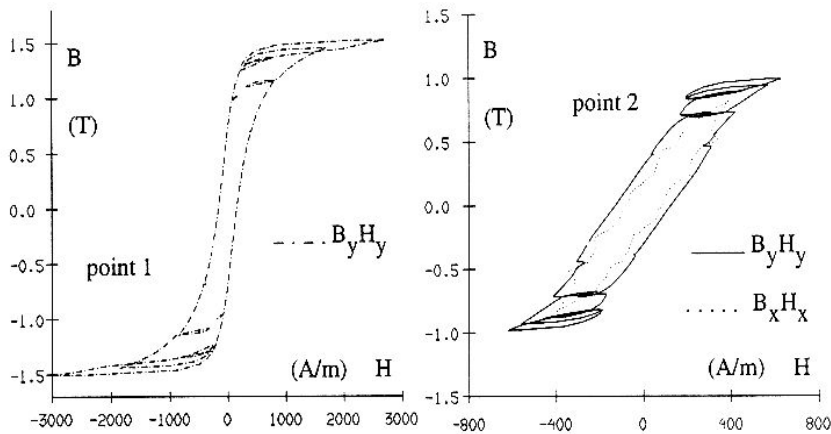


Figure 5.4: B_xH_x - and B_yH_y -loops in point 1 and point 2, case 2

We consider the 2 points indicated in Fig.5.1, for which we expect a different type of field pattern. The corresponding B_xH_x -loop and B_yH_y -loops are shown in Fig.5.4. For point 1, the B_xH_x -loop is omitted as, in correspondence with the alternating character of the flux pattern, $B_x \simeq H_x \simeq 0$. Fig.5.5 shows the *scaled* spectra of the amplitudes for the vectors \bar{B} and \bar{H} for point 1, according to (5.38)-(5.39).

Again the values obtained with the vector Preisach model deviates from those obtained with the single valued material characteristics (the more when the scaling factors are different, as indicated). Moreover, notice the symmetry for each pair of positive and negative harmonics. This corresponds to alternating field vectors, which is in agreement with a qualitative property for points such as point 1 in D . This symmetry is lost in the case of point 2 in D , see Fig.5.6, corresponding to rotational fields \bar{H} and \bar{B} in this point.

	$a_{j,1}$	$a_{j,15}$	$a_{j,17}$	$\gamma_{j,1}$	$\gamma_{j,15}$	$\gamma_{j,17}$
ϕ_1	1.262	0.0178	0.0105	25.	109.	-36.
ϕ_2	1.268	0.0067	0.0050	5.9	-155	27.

Table 2: amplitudes (1,2 and 3th column in Tesla) and angles (4,5 and 6th column in degrees) of the excitation in case 2, see formulas (5.42) and (5.43)

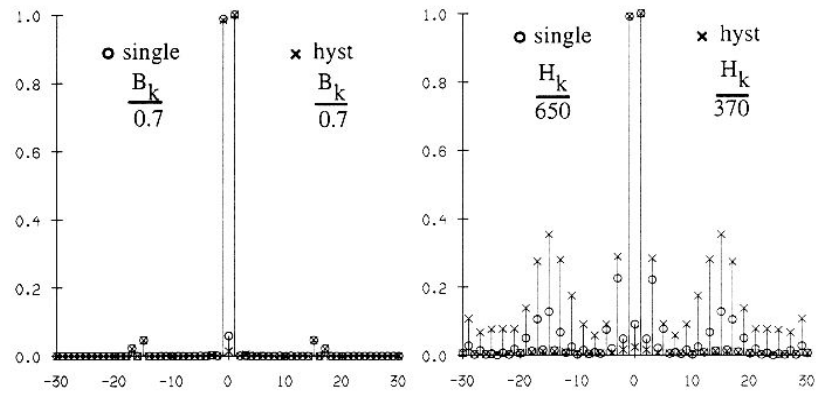


Figure 5.5: *Spectrum of the amplitude of \bar{B} and \bar{H} in point 1, case 2*

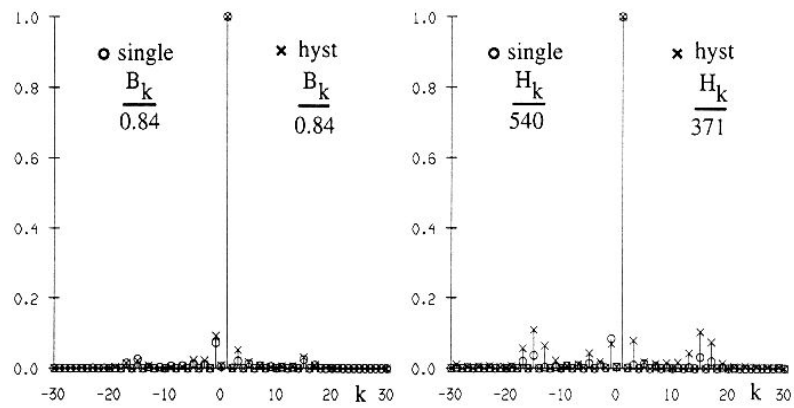


Figure 5.6: *Spectrum of the amplitude of \bar{B} and \bar{H} in point 2, case 2*

6 Concluding Remarks

In this paper we dealt with several types of nonlinear elliptic and parabolic BVPs with memory properties, both in 2D and 1D, in the former case with *nonlocal* BCs, arising e.g. from the mathematical modelling of the electromagnetic fields in magnetic materials with hysteresis behaviour. We presented effective numerical methods, proceeding in 3 steps: (1) a suitable (weak) variational formulation of the BVPs considered, (2) a nonstandard finite element method with quadratic elements w.r.t. the space dependency and (3) a time discretisation method of the Crank-Nicholson type, combined with Newton-Raphson iteration techniques. The major difficulty concerns the hysteresis behaviour of the material, reflected in the coefficient function (magnetic permeability) of the PDEs. The material models used are either scalar Preisach models (both rate-dependent and rate-independent) and a vector (rate-independent) Preisach model.

In the case of the scalar Preisach models the numerically obtained BH -loops and corresponding values of the electromagnetic losses agree with the experimental results, obtained by measurements. Actually, the material behaviour is described adequately by the material model. The calculations performed with the RPM are considerably more CPU-time consuming than those for the CPM, viz about 30 times more.

For the situations where the magnetic induction vector \bar{B} and the magnetic field vector \bar{H} are no longer uni-directional, a vector hysteresis model must be used. Although the vector Preisach theory has experimentally been found not to be adequate in all cases, this material model is the mostly elaborated and mostly used one in the literature. We have been able to incorporate it into the magnetic field calculations, although in a more complex way than for the scalar Preisach models. The combination of more refined vector hysteresis models, not available yet in the literature, with the magnetic field calculations will proceed along similar lines as in Sections 4-5.

The combined finite element - finite difference codes, which properly take into account the complex material behaviour in the BVPs considered, have been developed by the authors themselves, as the existing packages turned out not to be feasible, mainly due to that hysteresis behaviour.

Finally, we indicate some limitations of the paper and corresponding directions for further research. First, as emphasized from the beginning, in this article we restrict ourselves to BVPs in 1D and 2D, however showing *memory properties* (hysteresis) and, for the 2D-problem, showing also *nonlocal* BCs of the Neumann type. These 2 features make the BVPs nonstandard. In principle, 3D problems could be dealt with as well by the FEM-FDMs described, of course on the cost of higher computational complexity. However, as far as hysteresis models of Preisach-type are concerned, which must be coupled with the parabolic or elliptic problems, no thorough experimentally validated models in 3D exist (The mathematically much involved models developed by Mayergoyz, [14], for instance, are not really validated by measurements).

Other, more specific limitations concern the 2D-problems in Section 3 and 5. In

the underlying physical problems of Section 3 of electromagnetic field calculations in one lamination of an electric machine, the enforced flux is taken to be orthogonal to the cross section of both the yoke and the tooth, while in Section 5, the flux lies in the plane of the cross section, however with neglecting eddy current effects (i.e. $\bar{J} = 0$ in (1.43)). Without these physical assumptions the resulting BVPs are considerably more difficult. Thus, for instance, in Section 5, a scalar potential formulation would be no longer possible and, for the numerical approximation, the use of edge elements would be more appropriate than the one of finite elements. These extensions are topics for further research.

Acknowledgements

We would like to thank the Referee for his very valuable criticism, which has led to a considerable improvement of the paper, both in contents and in style of presentation. Luc Dupré is post-doctoral researcher of the Fund of Scientific Research - Flanders (F.W.O.).

References

- [1] M. Brokate and J. Sprekels, *Hysteresis and Phase Transitions*, Springer-Verlag, New York (1996).
- [2] P.G. Ciarlet and J.L. Lions (edits), *Finite Element Methods (Part 1)*, North-Holland, Amsterdam (1978).
- [3] J.T. Oden and J.N. Reddy, *An Introduction to the Mathematical Theory of Finite Elements*, J. Wiley, New York (1976).
- [4] P.A. Raviart and J.M. Thomas, *Introduction à l'analyse numérique des équations aux dérivées partielles (3^e tirage)*, Masson, Paris (1992).
- [5] D. Halliday and R. Resnick, *Fundamental of Physics*, John Wiley & Sons, New York (1981).
- [6] F. Preisach, Uber die magnetische Nachwirkung *Zeits. fur Physik*, **94** (1935) 277-302.
- [7] G. Bertotti, Dynamic Generalisation of the Scalar Preisach model of Hysteresis, *IEEE Trans. Magn.* **28** (1992) 2599-2601.
- [8] J-C. Bavay and J. Verdun, Alliages fer-silicium, *Technique de l'ingenieur D2-I* (1991) 2110-10.
- [9] D. Philips, L. Dupré and J. Melkebeek, Magneto-dynamic field computation using a rate-dependent Preisach model, *IEEE Trans. Magn.* **30** (1994) 4377-4379.

- [10] D. Jiles, A self Consistent Generalized Model for the Calculation of Minor Loop Excursions in the Theory of Hysteresis, *IEEE Trans. Magn.* **28** (1992) 2602-2604.
- [11] V. Ostovic, *Dynamics of Saturated Electric Machines*, Springer-Verlag, Berlin (1989).
- [12] L. Dupré, R. Van Keer and J. Melkebeek, On a Numerical Method for the Evaluation of Electromagnetic Losses in Electric Machinery, *Int. J. Num. Meth. Eng.* **39** (1996) 1535-1553.
- [13] D. Philips, L. Dupré, J. Cnops and J. Melkebeek, The Application of the Preisach Model in Magnetodynamics: Theoretical and Practical Aspects, *J. Magn. Mater.* **133** (1994) 540-543.
- [14] I.D. Mayergoyz, *Mathematical models of hysteresis*, Springer-Verlag, New York (1991).
- [15] I.D. Mayergoyz and G. Friedman, Isotropic vector Preisach model of hysteresis, *J. Appl. Phys.* **61** (1987) 4022-4024.

Roger Van Keer
Department of Mathematical Analysis,
University of Gent,
Galglaan 2, B-9000 Gent, Belgium

Luc Dupré
Department of Electrical Power Engineering,
University of Gent,
Sint-Pietersnieuwstraat 41, B-9000 Gent, Belgium